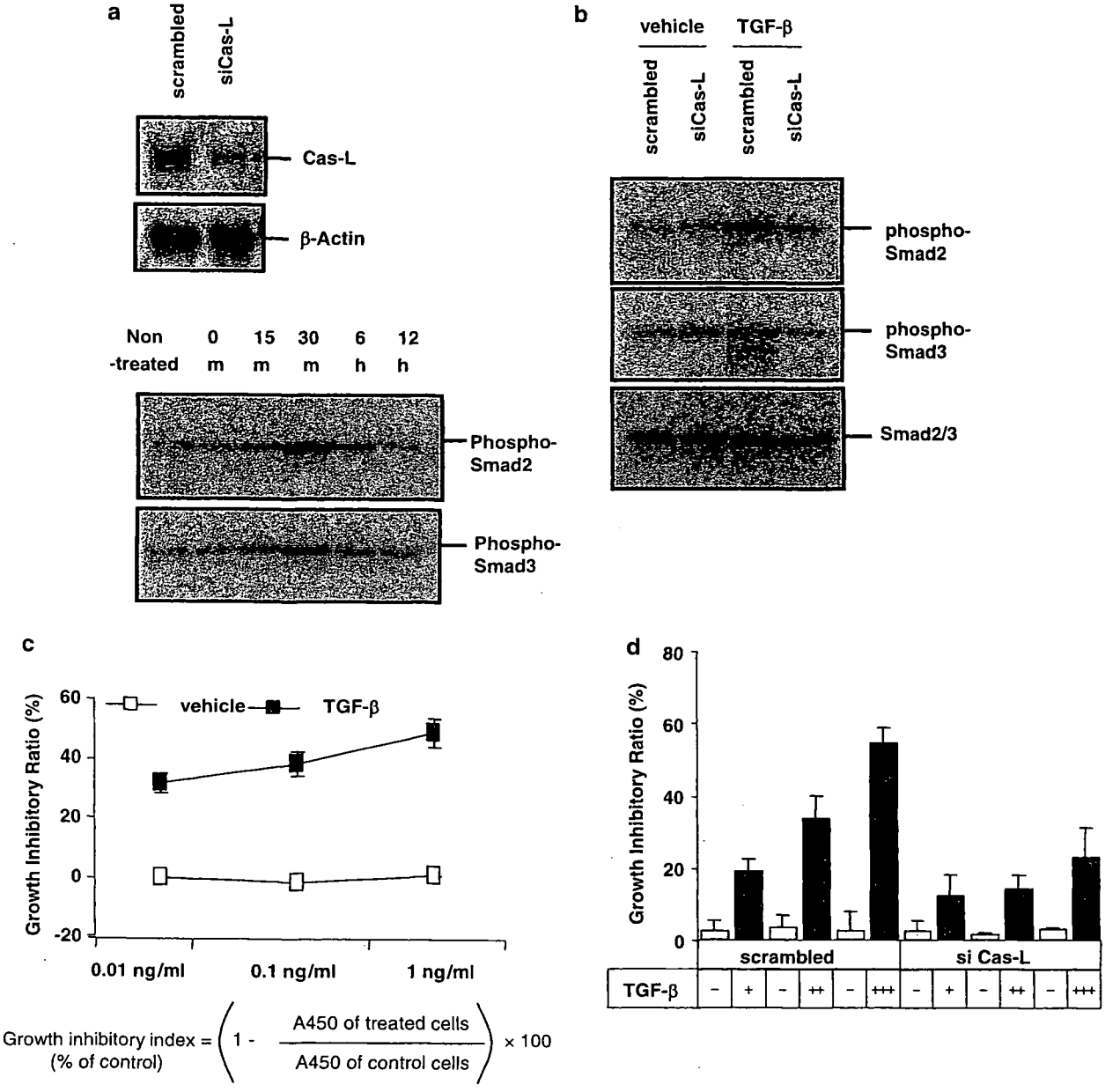

Figure 3 Depletion of Cas-L by siRNA oligo attenuates TGF-β signaling pathway. (a) Upper panel indicates the depletion of endogenous Cas-L in Huh-7 cells. Lower panel indicates time course study of phospho-Smad2 and phospho-Smad3 in TGF-β-treated Huh-7 cells. (b) In Huh-7 cells, phospho-Smad2 and phospho-Smad3 were assessed following TGF-β treatment in the presence of siCas-L or scrambled control. (c) Responsiveness of Huh-7 cells to TGF-β was assessed using *in vitro* proliferation assay. (d) Responsiveness of Huh-7 cells to TGF-β was assessed using *in vitro* proliferation assay with siCas-L or scrambled control.

Full length of Cas-L is necessary for the interaction with Smad6 or Smad7

Cas-L is a multifunctional docking protein with several domain structures specific for Cas family members. To define the particular domain structures of Cas-L necessary for the interaction with Smad6 or Smad7, deletion mutants of each domain or conserved motif of Cas-L protein were constructed. C-myc-tagged full-length Cas-L or mutant Cas-L cDNA subcloned into pEB6 vector was co-transfected with flag-tagged full-length Smad6 or Smad7 in 293 T cells. Full-length Cas-L (Cas-L wild type (wt)) co-precipitated with Smad6 (Figure 4a). Among the various mutants, only Cas-L F co-precipitated with Smad6 and Smad7, although its interaction with these proteins was weaker than Cas-L wt (Figure 4a and b). These results were verified by three independent tests, suggesting that the natural structure of Cas-L itself is necessary for its interaction with Smad6 or Smad7. Expanding on these results, each Cas-L mutant was tested for its effect on sensitivity to TGF-β using an *in vitro* proliferation model. Cas-L wt and Cas-L F enhanced sensitivity of Huh-7 cells to TGF-β, with other mutants and control vector having no effect (Figure 4c). Together with the immunoprecipitation

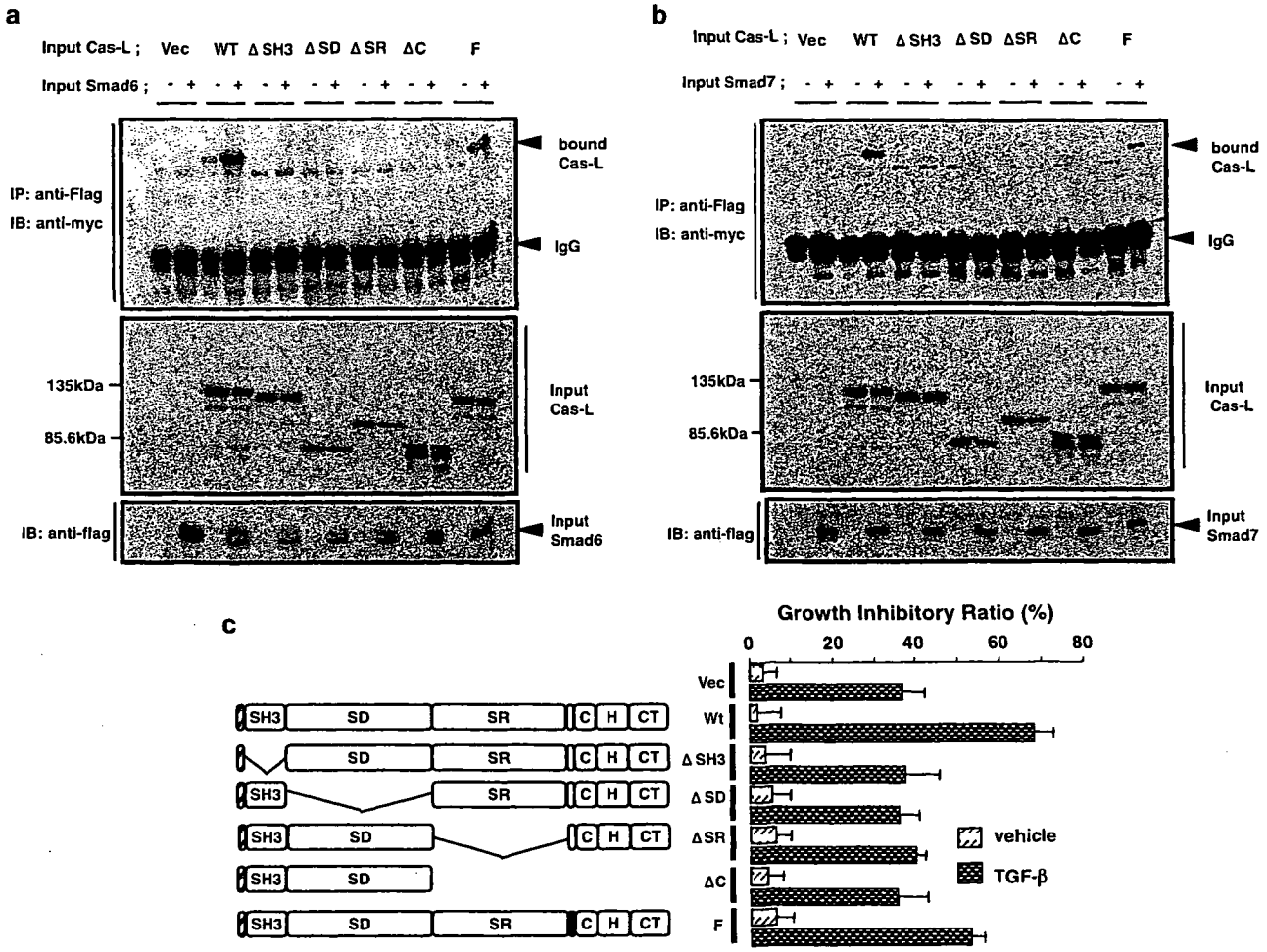

Figure 4 Full length of Cas-L is necessary for physical and functional interaction with Smad6 and Smad7. Each of c-myc tagged full-length Cas-L in a pEB6 vector (Cas-L wt), pEB6-c-myc-Cas-L ΔSH3 domain (Cas-L ΔSH3), pEB6-c-myc-CasL ΔSD domain (Cas-L ΔSD), pEB6-c-myc-CasL ΔSR domain (Cas-L ΔSR), pEB6-c-myc-Cas-L ΔC (Cas-L ΔC) and pEB6-c-myc-Cas-L F, in which Y629 and Y631 were mutated into F (Cas-L F) was co-transfected with pcDEF vector or pcDEF-flag-Smad6/7 in 293 T cells. (a) Lower panel indicates the input Smad6 revealed by immunoblotting using anti-flag antibody. Middle panel indicates the input Cas-L mutants revealed by immunoblotting using anti-c-myc antibody. Upper panel indicates the Cas-L mutants precipitated with Smad6. (b) Lower panel indicates the input Smad7 revealed by immunoblotting using anti-flag antibody. Middle panel indicates the input Cas-L mutants revealed by Western blotting using anti-c-myc antibody. Upper panel indicates the Cas-L mutants precipitated with Smad7. (c) Each Cas-L mutant was assessed for responsiveness of Huh-7 cells to 0.1 ng/ml TGF-β using *in vitro* proliferation assay.

results, these data clearly indicated that Cas-L F was weaker than Cas-L wt in its ability to enhance cellular sensitivity to TGF-β (Figure 4c), hence demonstrating the importance of the natural structure of Cas-L in its interaction with Smad6 or Smad7 and subsequent effect on TGF-β sensitivity.

Both C-terminal and N-terminal of Smad6 and Smad7 can interact with Cas-L

Smad6 and Smad7 have conserved domain structure, namely N-terminal Mad-homology (MH)1 domain and C-terminal MH2 domain (Figure 5a). We next employed flag-tagged Smad6 lacking MH1 domain (Smad6C), flag-tagged Smad6 lacking MH2 domain (Smad6N) and flag-tagged full-length Smad6 (Smad6F) in order to determine the binding domain of Smad6 to Cas-L. Smad7 mutants were also used in the same manner. C-myc-tagged Cas-L was co-precipitated with Smad6F, Smad6C and Smad6N. Likewise, Smad7F, Smad7C and Smad7N were all co-precipitated with Cas-L (Figure 5b).

To further explore the functional significance of the above results, Huh-7 cells co-transfected with mutants of I-Smads and pEB6 vector or Cas-L were subjected to *in vitro* proliferation assay with TGF-β. pEB6 vector plus Smad6F or Smad6C had weaker growth inhibitory effect than pEB6 vector plus pcDEF vector (Figure 5c, lanes 1, 3 and 5). Importantly, Cas-L plus pcDEF vector exhibited additive growth inhibitory effect (Figure 5c, lane 2). Moreover, Cas-L plus Smad6F or Smad6C counteracted the inhibitory effect of Smad6F or Smad6C on TGF-β-induced growth arrest (Figure 5c, lanes 4 and 6). It should be noted that the effect of Cas-L plus Smad6N did not differ from that of pEB6 plus Smad6N (Figure 5c, lanes 7 and 8), indicating that

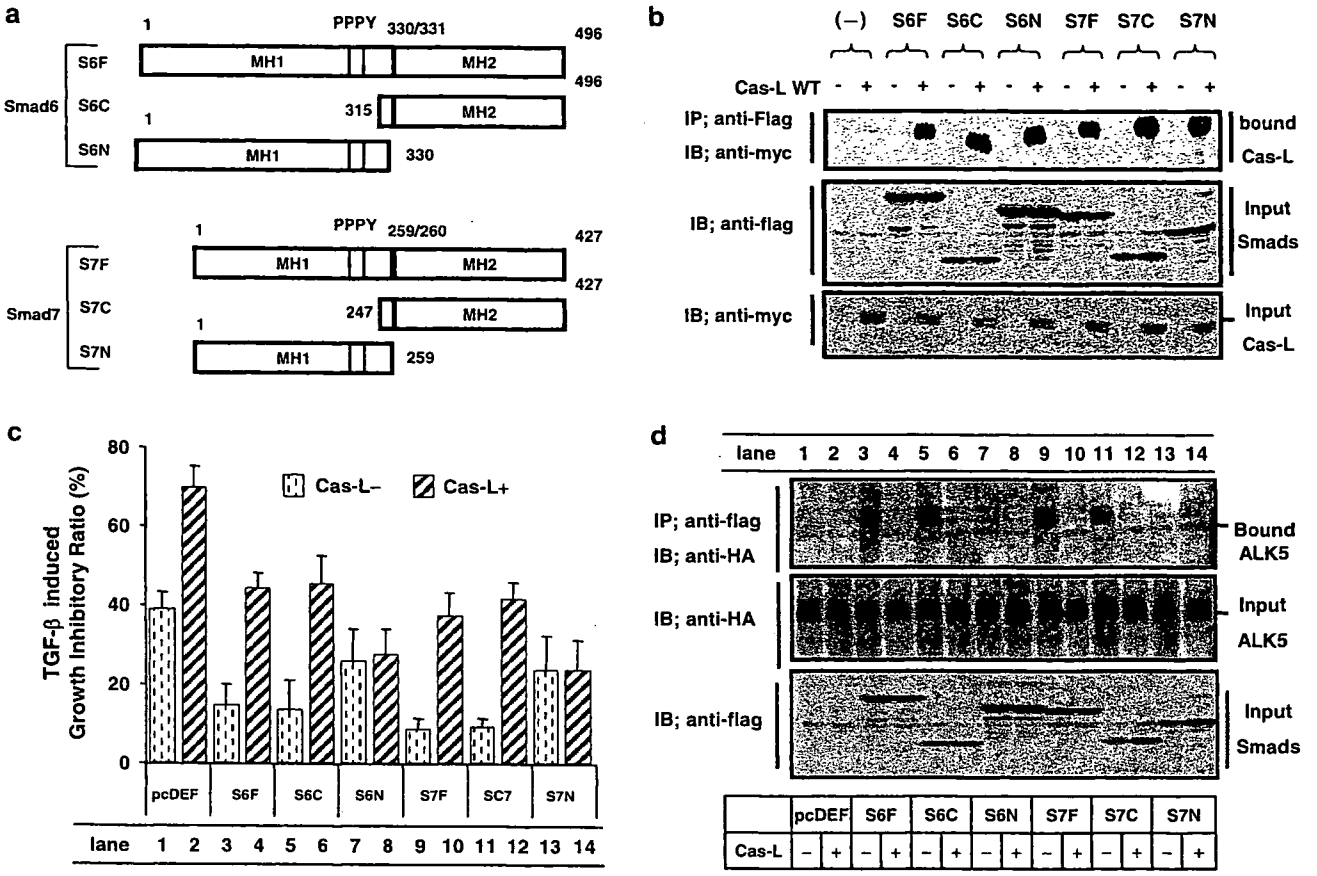

Figure 5 Cas-L interacts physically with MH1 and MH2 domain of Smad6 or Smad7, with MH2 domain playing a key role in TGF-β signaling pathway. (**a**) Flag tagged full-length Smad6 in a pcDEF6 vector (S6F), pcDEF-flag-Smad6 ΔN-terminal MH1 domain lacking aa 1–315 (S6C), pcDEF-flag-Smad6 ΔC-terminal MH2 domain lacking aa 331–496 (S6N), pcDEF-flag full-length Smad7 (S7F), pcDEF-flag-Smad7 ΔN-terminal MH1 domain lacking aa 1–247 (S7C), pcDEF-flag-Smad7 ΔC-terminal MH2 domain lacking aa 1–259 (S7C) was made. (**b**) Lower panel indicates the input full-length c-myc-Cas-L revealed by immunoblotting using anti-c-myc antibody. Middle panel indicates the input flag-Smad6/7 mutants revealed by immunoblotting using anti-flag antibody. Upper panel indicates the Cas-L mutants precipitated with Smad6/7 mutants. Host cell: 293 T cells. (**c**) Each Smad6/7 mutants was assessed in the presence or absence of full-length Cas-L for Huh-7 responsiveness to TGF-β. All mutants were treated with 0.1 ng/ml TGF-β for 24 h, and subsequently tested by *in vitro* proliferation assay. (**d**) Lower panel indicates the input flag-Smad6/7 mutants revealed by immunoblotting using anti-flag antibody. Middle panel indicates the input full-length HA-constitutively active ALK5 revealed by immunoblotting using anti-HA antibody. Upper panel indicates the Smads mutants precipitated with constitutively active ALK5 in the presence or absence of Cas-L. Host cell: 293 T cells.

the interaction between the C-terminal half of Smad6 and Cas-L is important in abrogating the inhibitory role of Smad6 on TGF-β signaling. Similar results were also obtained with the Smad7 model system (Figure 5c, lanes 9–14). These results suggested that Cas-L interacts with both the C-terminal and N-terminal domains of I-Smads, whereas the C-terminal but not the N-terminal of I-Smads has an important role in Cas-L-induced enhanced sensitivity to TGF-β.

Cas-L/C-terminal of I-Smads complex abrogates the recruitment of I-Smads to TGF-β type I receptor

N-terminal and C-terminal of I-Smads differ in their function in TGF-β signaling pathway, with the MH2 domain-containing C-terminal half of Smad6 and Smad7 being responsible for the interaction with TGF-β type I receptor that affects downstream activation of Smad2 and Smad3. Having demonstrated that I-Smads and Cas-L colocalized in the cytoplasm when pulsed by TGF-β (Figure 1c), we hypothesized that Cas-L/I-Smads interaction affects Smad6 or Smad7 binding to TGF-β type I receptor and subsequent inhibition of TGF-β signaling pathway. For this purpose, HA-tagged constitutively active ALK5 (TGF-β type I receptor) and Smad6 or Smad7 mutants were co-transfected into 293 cells. Smad6F, Smad6C, Smad7F and Smad7C were co-immunoprecipitated with constitutively active ALK5 (Figure 5d, lanes 3, 5, 9 and 11), but not Smad6N and Smad7N (Figure 5d, lanes 7, 8, 13 and 14), indicating that the C-terminal half of I-Smad is involved in receptor interaction. However, overexpression of Cas-L inhibited the interaction of I-Smads with constitutively active ALK5 (Figure 5d, lanes 4, 6, 10 and 12), indicating that Cas-L interferes with the association between TGF-β type I receptor and I-Smads.

Taken together, our results strongly suggested that Cas-L is a putative partner of I-Smads, and Cas-L/

I-Smad interaction, mediated by the C-terminal domain of I-Smads, abrogates the recruitment of I-Smads to TGF-β type I receptor, resulting in enhanced sensitivity to TGF-β signaling pathway (Figure 6a–c).

Discussion

In this report, we demonstrated that Cas-L interacts with two different I-Smads, Smad6 and Smad7, to counteract the antagonistic effect of I-Smads on TGF-β signaling. Furthermore, the attenuation of I-Smad function by Cas-L depends on interference with the recruitment of I-Smads to the TGF-β type I receptor.

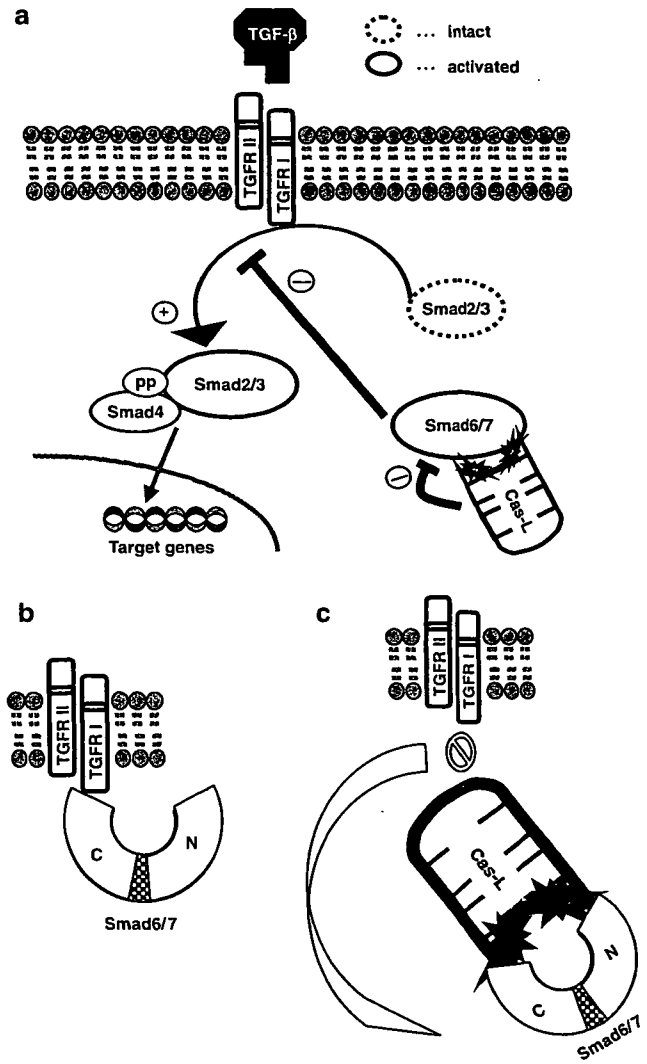

Figure 6 Schematic representation of Cas-L and Smad6/7 interaction. (**a**) TGF-β phosphorylates TGF type II and type I receptor, resulting in the activation of R-Smads, and subsequent homo- or hetero-dimerization with R-Smads or co-Smads. Heterodimerized Smads recruits into the nucleus, subsequently regulating transcriptional activity. I-Smads attenuate the activation of R-Smads. (**b** and **c**) Cas-L interacts with both of MH1 and MH2 domains of Smad6 and Smad7. MH2, but not MH1, domain contains the putative binding sites for the interaction with type I receptor. Cas-L interferes with type I receptor-associated recruiting of Smad6/7 by forming Cas-L–Smad6/7 complex.

Although TGF-β is reported to be a tumor suppressor during carcinogenesis, it also plays an opposite role in some tumors, depending on their origins and stages (Kato *et al.*, 2002). This finding suggests the existence of a cellular framework that allows for disruption of subcellular signaling molecules associated with TGF-β involvement in carcinogenesis. For example, certain gastrointestinal tumors have mutations in genes encoding components of the TGF-β signaling pathway, associated with aberrant growth of cancer cells. Defining the molecular basis for TGF-β unresponsiveness in tumors is therefore an important goal in further understanding cancer biology.

Our present work suggests that Cas-L activates TGF-β signaling pathway by interacting with the I-Smads, Smad6 and Smad7. Furthermore, Cas-L upregulates TGF-β-mediated transcriptional activity in gene reporter assays. Notably, genetically introduced Cas-L overcomes the Smad6 and Smad7-induced suppression of TGF-β-mediated SBE-luciferase reporter gene activity in 293 cells, suggesting that the underlying mechanism of Cas-L-induced sensitivity to TGF-β signaling is a loss of I-Smads function. Together with these results, overexpression of Cas-L protein results in an additive sensitivity to TGF-β. In support of this notion, depletion of Cas-L by siRNA oligo overcomes TGF-β-induced growth inhibition in Huh-7 cells, associated with decreased levels of TGF-β-induced phosphorylation of Smad2 and Smad3. Taken together, the above results strongly suggest that Cas-L is a positive regulator of TGF-β signaling.

Importantly, Cas-L interaction with Smad6 and Smad7 depends largely on the full integrity of its protein structure, as mutants lacking SH3 domain, substrate domain, serine-rich lesion and C-terminal all lose their binding affinity for Smad6 and Smad7, whereas only mutant whose Y629 and Y631 residues are mutated into F (FDFVHL) weakly interacts with Smad6 and Smad7. A unique aspect of our data is that the observed Cas-L/I-Smad interaction is not based on specific Cas-L domain, whereas other substrates for Cas-L, including FAK, Crk and Src, interact with its SH3 domain, substrate domain and YDYVHL motif, respectively (Tachibana *et al.*, 1997; Ohashi *et al.*, 1998). Additional supporting evidence is that only wt Cas-L, and not the mutants lacking the aforementioned domains, affects the sensitivity of Huh-7 cells to TGF-β. Of note is that the addition of the same mutant whose Y629 and Y631 residues are mutated into F (FDFVHL) retains cellular sensitivity to TGF-β.

Although Cas-L mutants except for Cas-L F do not bind to Smad6 and Smad7, all deletion mutants of Smad6 or Smad7 still retain their binding affinity to full-length Cas-L, suggesting that both MH1 and MH2 domains contain the binding motif for Cas-L. The fact that overexpressed Smad6 and Smad7 colocalize with Cas-L predominantly in the cytoplasm suggests that Cas-L/I-Smads interaction induces enhanced sensitivity to TGF-β outside the nucleus. Our work also indicates that Cas-L/I-Smads interaction influences the recruitment of I-Smads to TGF-β type I receptor. In the

absence of Cas-L, overexpressed constitutively active ALK5 (type I receptor) precipitates with full-length Smad6 and Smad7 and MH2 domain of Smad6 and Smad7, but not MH1 domain of Smad6 and Smad7, indicating that the MH2 domain contains the binding motif for ALK5. In the presence of Cas-L, full-length Smad6 and Smad7 and MH2 domain of Smad6 and Smad7 loses their binding affinity to ALK5, with MH1 domain of Smad6 and Smad7 still not binding to ALK5. These data thus indicate that Cas-L interferes with recruitment of Smad6 and Smad7 to TGF-β type I receptor via interaction with the MH2, but not MH1, domain of the I-Smads. Further experiments using affinity crosslinking by labeled TGF-β are being planned to clarify the interaction of I-Smads to TGF-β type I receptor.

A member of the Cas family proteins, which include p130Cas, Efs/Sin and Cas-L/HEF1, Cas-L has a described physiological role at focal adhesion sites (Ohashi *et al.*, 1998). Accumulating evidence strongly suggests that Cas-L is a multifunctional docking protein, with a role in cell motility (van Seventer *et al.*, 2001; Seo *et al.*, 2005), cytokine production (Kamiguchi *et al.*, 1999), cell shape change (Sasaki *et al.*, 2005), cell cycle (Astier *et al.*, 1997) and cell division (Pugacheva and Golemis, 2005), besides cell adhesion. Cas-L overexpression also induces apoptosis in HeLa cells, implying a potential role as a tumor suppressor (Law *et al.*, 2000). As tumor cells can develop resistance to TGF-β-mediated growth inhibition, it is conceivable that Cas-L plays a role in this process. We have found that several cancer cell lines exhibit profoundly impaired endogenous Cas-L (data not shown). In addition, previous work has reported that Huh-7 cells possessing detectable level of Cas-L protein are highly sensitive to TGF-β, whereas Jurkat cells possessing sparse level of Cas-L are not responsive to TGF-β treatment (Hayashi *et al.*, 1997; Lee *et al.*, 2002). It was previously shown that Cas-L binds to R-Smad, Smad3, with being proteasomally degraded by Smad3, and that overexpression of Cas-L in A549 cells results in inhibition of transcriptional activity in TGF-β signaling (Liu *et al.*, 2000). This discrepancy may be explained by that the cell type-specific abundance of subcellular downstream molecules in TGF-β signaling, including R-Smad/I-Smad ratio (Ito *et al.*, 2001), SARA (Xu *et al.*, 2000a) or Ski (Xu *et al.*, 2000b), which differently regulate TGF-β signaling in a complex manner. Moreover, previous work identified a splice variant of Smad6 that is differentially regulated in diseased tissues and appears to be a TGF-β pathway activator, in contrast to wt Smad6 (Krishnan *et al.*, 2001). Further studies are needed to examine the involvement of these molecules with Cas-L/I-Smads interaction in TGF-β signaling. Our data, together with previous work on TGF-β-mediated proteasomal degradation, suggest that the interaction of Cas-L with not only Smad3 but also Smad6 and Smad7, may be an essential part of an endogenous response aimed to limit the consequences of TGF-β refractoriness frequently observed in aggressive cancer cells.

In conclusion, our study indicates that Cas-L is a binding partner for Smad6 and Smad7, and that Cas-L potentiates TGF-β signaling mainly through its interaction with I-Smads. In view of the pivotal roles of TGF-β signaling in the pathophysiology of various diseases, studying Cas-L may therefore shed light on understanding the etiology of such conditions as cancer and connective tissue diseases.

Materials and methods

Reagents and antibodies

Rabbit polyclonal antibody against Cas-L was developed in our laboratory as described previously (Iwata *et al.*, 2005). Anti-c-myc tag monoclonal antibody (mAb) (9E10) was produced from the hybridoma obtained from the American Type Culture Collection (Manassas, VA, USA). Rabbit monoclonal antibodies to phosphorylated forms of Smad2 and Smad3, and mouse monoclonal antibodies to β-actin are all from Cell Signaling Technology Inc. (Beverly, MA, USA). Mouse monoclonal anti-Smad2/3 is from BD PharMingen (Lexington, KY, USA). Anti-Smad6 and Smad7 are from Santa Cruz Biotechnology (Santa Cruz, CA, USA).

Depletion of endogenous Cas-L

To deplete endogenous Cas-L, siRNA-oligo targeting Cas-L cDNA (accession no. NM_006403) was made according to the design site of TAKARA BIO (http://www.takara-bio.co.jp/RNAi.htm); sense: 5′-GGAUGGAUGACUACGAUUA TT-3′, antisense: 3′-TT CCUACCUACUGAUGCUAAU-5′, with its scrambled control oligo which contains the same GC quantity; sense: 5′-UAAUUAGGGUCGGGUAAAC TT-3′, antisense: 3′-TT AUUAAUCCCAGCCCAUUUG-5′. Cas-L siRNA oligo (siCas-L) was transfected using TransIT-TKO transfection reagent (Mirus Bio Corporation, Madison, WI, USA) according to the manufacturer's protocol.

Cells, plasmids and transfection procedures

Huh-7 cells (human hepatocellular carcinoma) were obtained from Cell Resource Center for Biomedical Research, Tohoku University, Sendai, Japan. 293 T cells were obtained from the American Type Culture Collection (Rockville, MD, USA). The plasmid vectors used in exploring signaling pathway were as follows: c-myc tagged full-length Cas-L in a pEB6 vector (Cas-L wt) (pEB6 vector is a kind gift from Y Miwa, University of Tsukuba, Tsukuba, Japan) (Tanaka *et al.*, 1999), pEB6-c-myc-Cas-L ΔSH3 domain lacking aa 1–60 (Cas-L ΔSH3), pEB6-c-myc-CasL ΔSD domain lacking aa 63–401 (Cas-L ΔSD), pEB6-c-myc-Cas-L ΔC lacking aa 406–834 (Cas-L ΔC) and pEB6-c-myc-Cas-L F, in which Y629 and Y631 were mutated into F (Cas-L F), respectively. pcDEF3-Flag (N)-Smad7 (aa 1–427), pcDEF3-Flag-Smad7C (aa 247–427), pcDEF3-Flag-Smad7N (aa 1–259), pcDEF3-Flag-Smad6 (aa 1–496), pcDEF3-Flag-Smad6C (aa 315-496), pcDEF3-Flag-Smad6N (aa 1–330) were provided by Kohei Miyazono as described previously (Hanyu *et al.*, 2001). The plasmids were transfected into cells using FuGENE6 reagent (Roche Diagnostics, Indianapolis, IN, USA).

Yeast two-hybrid screening

The two-hybrid analysis was carried out essentially as described previously (Iwata *et al.*, 2005), using pACTII (for GAL4 activator domain) (Li *et al.*, 1994) and pBTM116 (for LexA DNA-binding domain) (Vojtek *et al.*, 1993). The cDNA

encoding full-length Cas-L was subcloned into pBTM116. The resulting plasmid, pBTM116-Cas-L, was used as bait in a two-hybrid screen of a cDNA library of human HTLV-I infected T cell line (SLB-I) in *Saccharomyces cerevisiae* L40 according to the Matchmaker Two-Hybrid System Protocol (BD Biosciences Clontech, Palo Alto, CA, USA). Positive yeast clones were selected for histidine prototrophy and expression of β-gal. Plasmids containing cDNA clones were rescued from yeast and characterized by DNA sequencing. Concomitantly, those plasmids were introduced back to yeast strain L40 by a polyethylene glycol/lithium acetate method (Bartel *et al.*, 1993). Colonies were grown on selective synthetic medium and were examined for histidine prototrophy and β-gal activity.

In vitro *cell proliferation assay*
Cell proliferation assay was performed as described previously. In brief, cells were incubated in 96-well plates in media alone or in the presence of TGF-β (0.1, 1.0 or 10 ng/ml each) (R&D Systems, Minneapolis, MN, USA), or vehicle control for a total volume of 100 μl (5×10^3 cells/well). After 24 h of incubation at 37°C, Tetra Color ONE solution (Seikagaku, Tokyo, Japan) was added to each well. After another 2 h of incubation, fluorescence intensity was measured at 490 nm using a microplate reader (Bio-Rad, Hercules, CA, USA). All samples were tested in triplicate. Values represent the means of triplicate wells, and the s.e. of the mean was under 15%.

Immunocytochemistry
For fluorescent microscopy experiments using 293T cells, cells were treated and stained according to the methods described previously (Ohnuma *et al.*, 2004). In brief, 293T cells (5×10^4 cells/ml) were grown on coverslips in six-well plates, and transfected with c-myc-tagged Cas-L and Flag-tagged Smad6 or Smad7. The cells were fixed in 4% phosphate-buffered saline-paraformaldehyde solution for 15 min, followed by permeabilization with 0.1% Triton X-100 for 5 min. After blocking with TNB Blocking Buffer (TSA Fluorescence Systems, Perkin-Elmer Life Sciences, Boston, MA, USA), slips were stained with Cy3-labeled anti-c-myc mAb (Sigma, Saint Louis, MO, USA), and fluorescein isothiocynate (FITC)-labeled anti-Flag mAb (SIGMA) over night. After washing, slides were mounted with Prolong Antifade Kit (Molecular Probes, Eugene, OR, USA), and examined by confocal microscope with 40 objective lenses (IX70, Olympus, Tokyo, Japan) using laser excitation at 488 nm.

Immunoprecipitation, SDS–PAGE and immunoblotting
Protein (600 μg) from total cell lysates were diluted in the same final volume of NP-40 buffer (1% NP-40, 0.5% sodium deoxycholate, 5 mM ethylenediaminetetraacetic acid, 50 mM Tris-HCl (pH 8.0), 0.15 M NaCl), containing 1 mM phenylmethylsulfonyl fluoride (PMSF), 10 mM NaF, 1 mM Na_3VO_4, 10 μg/ml aprotinin and 10 μg/ml leupeptin. Corresponding antibodies were added at a final concentration of 2 μg/ml for immunoprecipitation, and immunoprecipitants were subjected to sodium dodecyl sulphate–polyacrylamide gel electrophoresis (SDS–PAGE) and immunoblotting. For detection of phosphorylated proteins, cells were harvested in NP-40 buffer containing 1 mM PMSF, 10 mM NaF, 1 mM Na_3VO_4, 10 μg/ml aprotinin and 10 μg/ml leupeptin. The protein samples were subjected to SDS–PAGE, transferred onto polyvinylidene difluoride membrane (Immobilon-P; Millipore, Bedford, MA, USA). Specific antigens were probed by the corresponding mAbs, followed by horseradish peroxidase conjugated anti-mouse immunoglobulin Ab (Amersham Pharmacia Biotech, Piscataway, NJ, USA). Western blots were visualized by the enhanced chemiluminescence technique (WESTERN LIGHTING, Chemiluminescence Reagent Plus, Perkin-Elmer Life Sciences, Boston, MA, USA).

Luciferase reporter assay
Luciferase reporter assay and transfection procedure were performed as described previously with some modification (Iwata *et al.*, 2005). Briefly, Dual-Luciferase Reporter Assay System (Promega, Madison, WI, USA) was used to measure luciferase activity expressed by the experimental plasmids. Cells were transfected with pWWP-Luc, p3TP-Lux (Cárcamo *et al.*, 1994) and pSBE-Luc using FuGENE6 reagent, according to the manufacturer's instructions. TGF-β was added 24 h after transfection. As internal control, renilla luciferase-expressing plasmid pRL-TK was employed. The enzyme activities of firefly luciferase and renilla luciferase were measured by Luminometer (Model TD-20/20, Turner Design, Inc., Sunnyvale, CA, USA).

Abbreviations

Cas-L, Crk-associated substrate lymphocyte type; TGF-β, transforming growth factor β.

Acknowledgements

This work was supported by Grant-in-Aid of Ministry of Education, Science, Sports and Culture (CM), and Ministry of Health, Labor, and Welfare, Japan (CM). T I is the recipients of a grant from Osaka Kidney Foundation (OKF05-0002), and The Yasuda Medical Foundation. We are thankful to Dr Takeshi Imamura (Department of Biochemistry, The JFCR Cancer Institute, Tokyo, Japan), and Dr Kohei Miyazono (Department of Molecular Pathology, Graduate School of Medicine, University of Tokyo, Japan) for providing us with constructs essential for the present work. We also thank Mr Hiroyuki Kayo for his technical assistance and advices.

References

Astier A, Manié SN, Law SF, Canty T, Haghayghi N, Druker BJ *et al.* (1997). Association of the Cas-like molecule HEF1 with CrkL following integrin and antigen receptor signaling in human B-cells: potential relevance to neoplastic lymphohematopoietic cells. *Leuk Lymphoma* **28**: 65–72.

Bartel P, Chien CT, Sternglanz R, Fields S. (1993). Elimination of false positives that arise in using the two-hybrid system. *Biotechniques* **14**: 920–924.

Cárcamo J, Weis FM, Ventura F, Wieser R, Wrana JL, Attisano L *et al.* (1994). Type I receptors specify growth-inhibitory and transcriptional responses to transforming growth factor beta and activin. *Mol Cell Biol* **14**: 3810–3821.

Chacko BM, Qin BY, Tiwari A, Shi G, Lam S, Hayward LJ *et al.* (2004). Structural basis of heteromeric smad protein assembly in TGF-beta signaling. *Mol Cell* **15**: 813–823.

Datta PK, Moses HL. (2000). STRAP and Smad7 synergize in the inhibition of transforming growth factor beta signaling. *Mol Cell Biol* **20**: 3157–3167.

Derynck R, Akhurst RJ, Balmain A. (2001). TGF-beta signaling in tumor suppression and cancer progression. *Nat Genet* **29**: 117–129.

Derynck R, Zhang YE. (2003). Smad-dependent and Smad-independent pathways in TGF-beta family signalling. *Nature* **425**: 577–584.

Fashena SJ, Einarson MB, O'Neill GM, Patriotis C, Golemis EA. (2002). Dissection of HEF1-dependent functions in motility and transcriptional regulation. *J Cell Sci* **115**: 99–111.

Grönroos E, Hellman U, Heldin CH, Ericsson J. (2002). Control of Smad7 stability by competition between acetylation and ubiquitination. *Mol Cell* **10**: 483–493.

Hanyu A, Ishidou Y, Ebisawa T, Shimanuki T, Imamura T, Miyazono K. (2001). The N domain of Smad7 is essential for specific inhibition of transforming growth factor-beta signaling. *J Cell Biol* **155**: 1017–1027.

Hayashi H, Abdollah S, Qiu Y, Cai J, Xu YY, Grinnell BW *et al.* (1997). The MAD-related protein Smad7 associates with the TGFbeta receptor and functions as an antagonist of TGFbeta signaling. *Cell* **89**: 1165–1173.

Heldin CH, Miyazono K, ten Dijke P. (1997). TGF-beta signalling from cell membrane to nucleus through SMAD proteins. *Nature* **390**: 465–471.

Hynes RO. (1992). Integrins: versatility, modulation, and signaling in cell adhesion. *Cell* **69**: 11–25.

Ito Y, Zhao J, Mogharei A, Shuler CF, Weinstein M, Deng C *et al.* (2001). Antagonistic effects of Smad2 versus Smad7 are sensitive to their expression level during tooth development. *J Biol Chem* **276**: 44163–44172.

Iwata S, Souta-Kuribara A, Yamakawa A, Sasaki T, Shimizu T, Hosono O *et al.* (2005). HTLV-I Tax induces and associates with Crk-associated substrate lymphocyte type (Cas-L). *Oncogene* **24**: 1262–1271.

Juliano RL, Haskill S. (1993). Signal transduction from the extracellular matrix. *J Cell Biol* **120**: 577–585.

Kamiguchi K, Tachibana K, Iwata S, Ohashi Y, Morimoto C. (1999). Cas-L is required for beta 1 integrin-mediated costimulation in human Tcells. *J Immunol* **163**: 563–568.

Kato Y, Habas R, Katsuyama Y, Näär AM, He X. (2002). A component of the ARC/Mediator complex required for TGF beta/Nodal signalling. *Nature* **418**: 641–646.

Krishnan P, King MW, Neff AW, Sandusky GE, Bierman KL, Grinnell B *et al.* (2001). Human truncated Smad 6 (Smad 6s) inhibits the BMP pathway in *Xenopus laevis*. *Dev Growth Differ* **43**: 115–132.

Law SF, Estojak J, Wang B, Mysliwiec T, Kruh G, Golemis EA. (1996). Human enhancer of filamentation 1, a novel p130cas-like docking protein, associates with focal adhesion kinase and induces pseudohyphal growth in *Saccharomyces cerevisiae*. *Mol Cell Biol* **16**: 3327–3337.

Law SF, O'Neill GM, Fashena SJ, Einarson MB, Golemis EA. (2000). The docking protein HEF1 is an apoptotic mediator at focal adhesion sites. *Mol Cell Biol* **20**: 5184–5195.

Lee HY, Chun KH, Liu B, Wiehle SA, Cristiano RJ, Hong WK *et al.* (2002). Insulin-like growth factor binding protein-3 inhibits the growth of non-small cell lung cancer. *Cancer Res* **62**: 3530–3537.

Li L, Elledge SJ, Peterson CA, Bales ES, Legerski RJ. (1994). Specific association between the human DNA repair proteins XPA and ERCC1. *Proc Natl Acad Sci USA* **91**: 5012–5016.

Liu X, Elia AE, Law SF, Golemis EA, Farley J, Wang T. (2000). A novel ability of Smad3 to regulate proteasomal degradation of a Cas family member HEF1. *EMBO J* **19**: 6759–6769.

Minegishi M, Tachibana K, Sato T, Iwata S, Nojima Y, Morimoto C. (1996). Structure and function of Cas-L, a 105-kD Crk-associated substrate-related protein that is involved in beta 1 integrin-mediated signaling in lymphocytes. *J Exp Med* **184**: 1365–1375.

Miyake-Nishijima R, Iwata S, Saijo S, Kobayashi H, Kobayashi S, Souta-Kuribara A *et al.* (2003). Role of Crk-associated substrate lymphocyte type in the pathophysiology of rheumatoid arthritis in tax transgenic mice and in humans. *Arthritis Rheum* **48**: 1890–1900.

Nakao A, Afrakhte M, Morén A, Nakayama T, Christian JL, Heuchel R *et al.* (1997). Identification of Smad7, a TGFbeta-inducible antagonist of TGF-beta signalling. *Nature* **389**: 631–635.

Ohashi Y, Iwata S, Kamiguchi K, Morimoto C. (1999). Tyrosine phosphorylation of Crk-associated substrate lymphocyte-type is a critical element in TCR- and beta 1 integrin-induced T lymphocyte migration. *J Immunol* **163**: 3727–3734.

Ohashi Y, Tachibana K, Kamiguchi K, Fujita H, Morimoto C. (1998). T cell receptor-mediated tyrosine phosphorylation of Cas-L, a 105-kDa Crk-associated substrate-related protein, and its association of Crk and C3G. *J Biol Chem* **273**: 6446–6451.

Ohnuma K, Yamochi T, Uchiyama M, Nishibashi K, Yoshikawa N, Shimizu N *et al.* (2004). CD26 up-regulates expression of CD86 on antigen-presenting cells by means of caveolin-1. *Proc Natl Acad Sci USA* **101**: 14186–14191.

Pugacheva EN, Golemis EA. (2005). The focal adhesion scaffolding protein HEF1 regulates activation of the Aurora-A and Nek2 kinases at the centrosome. *Nat Cell Biol* **7**: 937–946.

Sasaki T, Iwata S, Okano HJ, Urasaki Y, Hamada J, Tanaka H *et al.* (2005). Nedd9 protein, a Cas-L homologue, is upregulated after transient global ischemia in rats: possible involvement of Nedd9 in the differentiation of neurons after ischemia. *Stroke* **36**: 2457–2462.

Seo S, Asai T, Saito T, Suzuki T, Morishita Y, Nakamoto T *et al.* (2005). Crk-associated substrate lymphocyte type is required for lymphocyte trafficking and marginal zone B cell maintenance. *J Immunol* **175**: 3492–3501.

Sugano Y, Matsuzaki K, Tahashi Y, Furukawa F, Mori S, Yamagata H *et al.* (2003). Distortion of autocrine transforming growth factor beta signal accelerates malignant potential by enhancing cell growth as well as PAI-1 and VEGF production in human hepatocellular carcinoma cells. *Oncogene* **22**: 2309–2321.

Tachibana K, Urano T, Fujita H, Ohashi Y, Kamiguchi K, Iwata S *et al.* (1997). Tyrosine phosphorylation of Crk-associated substrates by focal adhesion kinase. A putative mechanism for the integrin-mediated tyrosine phosphorylation of Crk-associated substrates. *J Biol Chem* **272**: 29083–29090.

Tanaka J, Miwa Y, Miyoshi K, Ueno A, Inoue H. (1999). Construction of Epstein–Barr virus-based expression vector containing mini-oriP. *Biochem Biophys Res Commun* **264**: 938–943.

van Seventer GA, Salmen HJ, Law SF, O'Neill GM, Mullen MM, Franz AM *et al.* (2001). Focal adhesion kinase regulates beta1 integrin-dependent T cell migration through an HEF1 effector pathway. *Eur J Immunol* **31**: 1417–1427.

Vojtek AB, Hollenberg SM, Cooper JA. (1993). Mammalian Ras interacts directly with the serine/threonine kinase Raf. *Cell* **74**: 205–214.

Xu L, Chen YG, Massagué J. (2000a). The nuclear import function of Smad2 is masked by SARA and unmasked by TGFbeta-dependent phosphorylation. *Nat Cell Biol* **2**: 559–562.

Xu W, Angelis K, Danielpour D, Haddad MM, Bischof O, Campisi J *et al.* (2000b). Ski acts as a co-repressor with Smad2 and Smad3 to regulate the response to type beta transforming growth factor. *Proc Natl Acad Sci USA* **97**: 5924–5929.

Yagil C, Hubner N, Monti J, Schulz H, Sapojnikov M, Luft FC *et al.* (2005). Identification of hypertension-related genes through an integrated genomic-transcriptomic approach. *Circ Res* **96**: 617–625.

Zhang Z, Baron R, Horne WC. (2000). Integrin engagement, the actin cytoskeleton, and c-Src are required for the calcitonin-induced tyrosine phosphorylation of paxillin and HEF1, but not for calcitonin-induced Erk1/2 phosphorylation. *J Biol Chem* **275**: 37219–37223.

Supplementary Information accompanies the paper on the Oncogene website (http://www.nature.com/onc).

Anti-CD26 Monoclonal Antibody–Mediated G_1-S Arrest of Human Renal Clear Cell Carcinoma Caki-2 Is Associated with Retinoblastoma Substrate Dephosphorylation, Cyclin-Dependent Kinase 2 Reduction, $p27^{kip1}$ Enhancement, and Disruption of Binding to the Extracellular Matrix

Teruo Inamoto,[1,3] Tadanori Yamochi,[1] Kei Ohnuma,[1] Satoshi Iwata,[1] Shinichiro Kina,[1] Sakiko Inamoto,[1,3] Masaaki Tachibana,[2] Yoji Katsuoka,[3] Nam H. Dang,[4] and Chikao Morimoto[1,4]

Abstract **Purpose:** CD26 is a 110-kDa cell surface glycoprotein with a role in tumor development through its association with key intracellular proteins. In this report, we show that binding of soluble anti-CD26 monoclonal antibody (mAb) inhibits the growth of the human renal carcinoma cells in both *in vitro* and *in vivo* experiments.

Experimental Design: Growth inhibition by anti-CD26 mAb was assessed using proliferation assay and cell cycle analysis. Anti-CD26 mAb, chemical inhibitors, dominant-negative, or constitutively active forms of specific signaling molecules were used to evaluate CD26-associated pathways. The *in vivo* growth-inhibitory effect of anti-CD26 mAb was also assessed in a human renal carcinoma mouse xenograft model.

Results: *In vitro* experiments show that anti-CD26 mAb induces G_1-S cell cycle arrest associated with enhanced $p27^{kip1}$ expression, down-regulation of cyclin-dependent kinase 2, and dephosphorylation of retinoblastoma substrate. Moreover, our data show that enhanced $p27^{kip1}$ expression is dependent on the attenuation of Akt activity. Anti-CD26 mAb also internalizes cell surface CD26, leading to decreased binding to collagen and fibronectin. Experiments with a mouse xenograft model involving human renal carcinoma cells show that anti-CD26 mAb treatment drastically inhibits tumor growth in tumor-bearing mice, resulting in enhanced survival.

Conclusions: Taken together, our data strongly suggest that anti-CD26 mAb treatment may have potential clinical use for CD26-positive renal cell carcinomas.

CD26 is a 110-kDa surface glycoprotein with dipeptidyl peptidase IV activity able to cleave selected biological factors to alter their functions (1). CD26/dipeptidyl peptidase IV is involved in T lymphocyte signal transduction processes (2, 3) and regulates topoisomerase IIα level in hematologic malignancies, affecting sensitivity to doxorubicin and etoposide (4). Moreover, our previous work showed that anti-CD26 monoclonal antibody (mAb) inhibits growth of CD26-positive T-cell malignancies (5, 6). Expressed on various tissues, including epithelial cells of liver, intestine, and kidney (1, 7), CD26 is involved in the development of certain human cancers, with lung adenocarcinomas, differentiated thyroid carcinomas, and metastatic prostate cancer being CD26 high and other histologic types of lung carcinomas, benign thyroid diseases, and primary prostate cancer being CD26 low (7–10). Notably, the role of CD26 in cancer biology depends on tumor types, as it is associated with high level of tumor aggressiveness in some and lower level in others (7–10). In a previous report, CD26 expression was detected on renal cell carcinoma (RCC) with unclear clinical significance (11). Extending these previous findings, we now define CD26 expression on normal and malignant tubular epithelial kidney tissues and establish that CD26 is an appropriate target for RCC treatment.

CD26 structure consists of three regions, an extracellular region, a 22-residue hydrophobic transmembrane region, and a 6-amino acid cytoplasmic region. The extracellular region contains a membrane-proximal glycosylated domain, a cysteine-rich domain, and a 260-amino acid COOH-terminal domain containing dipeptidyl peptidase IV activity. We now

Authors' Affiliations: [1]Division of Clinical Immunology, Advanced Clinical Research Center, Institute of Medical Science, University of Tokyo; [2]Department of Urology, Tokyo Medical College, Tokyo, Japan; [3]Department of Urology, Osaka Medical College, Osaka, Japan; and [4]Department of Hematologic Malignancies, Nevada Cancer Institute, Las Vegas, Nevada

Received 2/16/06; revised 3/22/06; accepted 3/29/06.

Grant support: Grant-in-Aid of Ministry of Education, Science, Sports, and Culture (K. Ohnuma and C. Morimoto) and Ministry of Health, Labor, and Welfare, Japan (C. Morimoto); Osaka Kidney Foundation grant OKF05-0002 (T. Inamoto); and The Yasuda Medical Foundation.

The costs of publication of this article were defrayed in part by the payment of page charges. This article must therefore be hereby marked *advertisement* in accordance with 18 U.S.C. Section 1734 solely to indicate this fact.

Requests for reprints: Chikao Morimoto, Division of Clinical Immunology, Advanced Clinical Research Center, Institute of Medical Science, University of Tokyo, 4-6-1, Shirokanedai, Minato-ku, Tokyo 108-8639, Japan. Phone: 81-3-5449-5549; Fax: 81-3-5449-5548; E-mail: morimoto@ims.u-tokyo.ac.jp.

doi:10.1158/1078-0432.CCR-06-0361

show that the anti-CD26 mAb 14D10, which recognizes the cell membrane-proximal glycosylated region starting with a 20-amino acid flexible stalk region of human CD26, induces cell cycle arrest, concomitantly blocking the adhesion of RCC cells to the extracellular matrix (ECM). In addition, anti-CD26 mAb-mediated growth arrest of RCC cells results from dephosphorylation of retinoblastoma substrate, decreased level of cyclin-dependent kinase (CDK) 2, and up-regulation of the Akt-dependent CDK inhibitor $p27^{kip1}$. Furthermore, studies using a mouse xenograft model show that anti-CD26 mAb treatment inhibits RCC tumor growth *in vivo*. Our work hence suggests a potential role for CD26-targeted therapy in the treatment of human RCC.

Materials and Methods

Reagents and antibodies. Anti-CD26 mAb (IgG1) 14D10 and anti-CD45 mAb (IgG1) 2H4 were developed in our laboratory as described previously (12, 13), with the latter being used as isotype-matched control mAb. Rabbit mAb to Thr^{308} or Ser^{473}-phosphorylated forms of Akt and phosphorylated extracellular signal-regulated kinase (ERK) 1/2 and mouse mAb to protein kinase Bα/Akt, ERK1/2, CDK4, CDK6, and phosphothreonine were from Cell Signaling Technology, Inc. (Beverly, MA), and mouse mAb to $p21^{cip1/waf1}$, CDK2, p53, cyclin D1, retinoblastoma substrate, and $p27^{kip1}$ were from BD PharMingen (Lexington, KY). Oct-1, and α-tubulin were from Santa Cruz Biotechnology (Santa Cruz, CA). LY294002, wortmannin, and PD98059 were from Calbiochem (San Diego, CA). Nocodazole was from Sigma-Aldrich (St. Louis, MO). Nocodazole (500 ng/mL from 1 mg/mL stock solution in DMSO), LY294002 (30 μmol/L from 50 mmol/L stock solution in DMSO), and PD98059 (30 μmol/L from 10 mmol/L stock solution in DMSO) were added to the culture medium 30 minutes before treatment with each antibody.

Cell culture and transfection procedures. Caki-2 (human renal carcinoma), LNCap (androgen-dependent prostate carcinoma), and DU-145 cells (androgen-independent prostate carcinoma) were kind gifts from Dr. Haruhito Azuma (Osaka Medical College, Osaka, Japan). VMRC-RCW (human renal carcinoma), Caki-1 (human renal carcinoma), and ACHN (human renal carcinoma) were obtained from Cell Resource Center for Biomedical Research (Tohoku University, Sendai, Japan). All cells were grown in RPMI 1640 (Life Technologies, Inc., Grand Island, NY) supplemented with 10% heat-inactivated fetal bovine serum, penicillin (100 units/mL), and streptomycin (100 μg/mL; Life Technologies, Inc., Gaithersburg, MD) or G418 (500 μg/mL; Sigma-Aldrich). The plasmid vectors (Upstate Biotechnology, Lake Placid, NY) used in exploring signaling pathway were as follows: the Myc-tagged NH_2-terminal myristylated active Akt1 cDNA (Myr-Akt), dominant-negative form of Akt cDNA (d.n.-Akt), and hemagglutinin-tagged constitutive active mitogen-activated protein kinase (MAPK)/ERK kinase (MEK) 1 cDNA (upstream of 44/42MAPK; c.a. MEK1), with all three constructs being placed in a pUSEamp vector. The plasmids were transfected into various cells using Fugene 6 reagent (Roche Diagnostics, Indianapolis, IN). In each experiment, neomycin phosphotransferase II (Upstate Biotechnology) was probed to evaluate transfection efficacy.

Cell cycle analyses. Cells (1×10^6 per well) were incubated in medium alone or in the presence of anti-CD26 or isotype-matched control mAbs at indicated concentrations in the presence or absence of nocodazole. DNA contents were analyzed using propidium iodide as described previously (5) and were measured using FACSCalibur (Becton Dickinson Co., San Jose, CA) with CellQuest software (Becton Dickinson) and ModFit program (Becton Dickinson). In all experiments, at least $>1 \times 10^4$ cells were sorted after gating out the fixation artifacts and cell debris.

2-(2-Methoxy-4-nitrophenyl)-3-(4-nitrophenyl)-5-(2,4-disulfophenyl)-2H-tetrazolium assay. Cells were synchronized using double-thymidine block method as described previously (14), then released, and subjected to incubation in 96-well plates in medium alone or in the presence of anti-CD26 (0.1, 1, or 10 μg/mL) or isotype-matched control mAbs (0.1, 1, or 10 μg/mL) for a total volume of 100 μL (5×10^3 cells per well). After 24 hours of incubation in 37°C, 2-(2-methoxy-4-nitrophenyl)-3-(4-nitrophenyl)-5-(2,4-disulfophenyl)-2H-tetrazolium (Seikagaku, Tokyo, Japan) was added to each well. After another 2 hours of incubation, water-soluble formazan dye on bioreduction in the presence of an electron carrier, 1-methoxy-5-methylphenazinium, was measured at 450 nm using a microplate reader (Bio-Rad, Hercules, CA). All samples were tested in triplicate. Values reported represent the mean of triplicated wells, and SE was within 15%.

Immunocytochemistry and immunohistochemistry. For fluorescent microscopy experiments, cells were treated and stained according to the methods described previously (3). In brief, Caki-2 cells (5×10^4/mL) were grown on coverslips in six-well plates in the presence or absence of anti-CD26 mAb. The cells were fixed in 4% paraformaldehyde followed by permeabilization with 0.1% Triton X-100 in PBS and stained with anti-$p27^{kip1}$ mAb and FITC-conjugated anti-mouse IgG (Jackson ImmunoResearch, West Grove, PA). After mounting with a ProLong Antifade kit (Molecular Probes, Eugene, OR), slides were examined by Olympus IX70 confocal microscope with 40 objective lenses (Olympus, Tokyo, Japan) using laser excitation at 488 nm. For immunohistochemistry, 11 primary RCC surgical specimens from patients were evaluated. For each, 10% formalin-fixed, paraffin-embedded specimens containing both the carcinoma and its adjacent nonneoplastic tissue were prepared. Slides were deparaffinized and then heated in a microwave processor for antigen retrieval in 10 mmol/L citrate buffer (pH 6) for 10 minutes. After blocking in 3% (v/v) bovine serum albumin, slides were incubated at 4°C overnight with the primary antibody (anti-CD26 mAb), washed with PBS, incubated for 30 minutes with FITC-conjugated anti-mouse IgG, and then analyzed using confocal laser microscopy. To serve as a control for nonspecific staining, duplicate sections were stained with isotype-matched mAb instead of the primary antibody. Two different pathologists checked the validity of the obtained results. All human specimens were obtained from the Department of Urology, Tokyo Medical College (Tokyo, Japan), and informed consents were obtained from all patients according to the format of the Institutional Review Board.

SDS-PAGE and immunoblotting. Preparation of whole-cell lysates and cell fractionations were done as described elsewhere (15). For detection of phosphorylated proteins, cells were harvested in NP40 buffer [1% NP40, 0.5% sodium deoxycholate, 5 mmol/L EDTA, 50 mmol/L Tris-HCl (pH 8), 0.15 mol/L NaCl] containing 1 mmol/L phenylmethylsulfonyl fluoride, 10 mmol/L NaF, 1 mmol/L Na_3VO_4, 10 μg/mL aprotinin, and 10 μg/mL leupeptin. The protein samples were subjected to SDS-PAGE and transferred to polyvinylidene difluoride membrane (Immobilon-P, Millipore, Bedford, MA). Specific antigens were probed by the corresponding mAbs followed by horseradish peroxidase-conjugated secondary Ig (Amersham Pharmacia Biotech, Piscataway, NJ). Western blots were visualized by the enhanced chemiluminescence technique (NEN, Boston, MA).

In vivo *model.* *In vivo* studies were approved by the Institute Animal Care and Use Committee. Female-specific pathogen-free BALB/c nu−/− mice (ages 8 weeks) were purchased from Charles River (Yokohama, Japan). All mice were pretreated by i.p. route with 0.2 mL anti-asialo-GM1 polyclonal antisera (25%, v/v; Wako, Osaka, Japan) 1 day before tumor transplant to eliminate host natural killer cell activity. For a xenograft model of RCC, mice were anesthetized with diethyl ether and subjected to direct s.c. inoculation of Caki-2 cells (1×10^6 per mouse) in 100 μL Matrigel (BD Biosciences, San Jose, CA). The studies involving the observation of tumor volume and survival advantage included five mice per group. Mice bearing established tumors (~5 mm in size) received PBS alone, anti-CD26 mAb, or isotype-matched control mAb by intratumoral injection in 0.1-mL volume of sterile PBS at 10 μg per

dose as described previously (6). The mice were injected every 4 days for 60 days. Tumor-bearing mice were then monitored for tumor development and progression. Tumor size was determined by caliper measurement of the largest (x) and smallest (y) perpendicular diameters every 4 days and calculated according to the formula $V = \pi/6 \times xy^2$. Cumulative proportion survival was assessed by Kaplan-Meier. Necropsies of moribund mice were done for evaluation of tumor, and tumors were removed to be frozen. After homogenization by Dounce homogenizer, frozen tissues were lysed in lysis buffer [1% SDS, 4 mol/L urea, 1 mmol/L EDTA, 150 mmol/L NaCl, 50 mmol/L Tris (pH 8)]. Each 50 μg of lysates was subjected to SDS-PAGE and immunoblotting to examine protein levels of $p27^{kip1}$, phosphorylated Akt, and β-actin.

Results

Cell surface CD26 is highly expressed on human RCC. Previous work showed CD26 expression is enhanced on RCC (11). We first evaluated CD26 expression level on surgically resected human RCC tissues from Japanese patients. Eleven consecutive surgically resected RCC specimens from the primary sites were examined for surface CD26 expression. CD26 was highly expressed on RCC tissues compared with normal renal cells surrounding the RCC (Fig. 1A, *a* and *b*) particularly in normal proximal tubules (Fig. 1A, *c* and *d*). All 11 RCC tissues and 6 normal renal tissues surrounding RCC were evaluated for their CD26 expression intensity, revealing high expression on human RCC tissues compared with normal renal tissues (Fig. 1B). The RCC cell lines Caki-2, VMRC-RCW, Caki-1, and ACHN all exhibited high surface CD26 levels, with DU-145 and LNCap showing much lower expression (Fig. 1C). These data indicated that all RCC cells tested were highly CD26 positive, whereas tumor cells arising from other origins, including prostate cancers, exhibited much lower level.

Anti-CD26 mAb induces cell cycle arrest at G_1-S checkpoint and growth inhibition of RCC. Because we showed previously that anti-CD26 mAb treatment induced cell cycle arrest at G_1-S in CD26-positive T-cell lymphoma and T-cell clones (5, 6), we first examined anti-CD26 mAb effect on cell cycle progression of CD26-positive RCC cell lines. Treatment of Caki-2 cells with anti-CD26 blocked cell cycle progression at G_1-S (Fig. 2A), an effect better visualized when cells were treated with nocodazole to induce M-phase cell cycle arrest (Fig. 2B). Caki-2 cells exhibited a significant increase in G_0-G_1 from 14 to 28 hours after initiation of anti-CD26 treatment (Fig. 2C), whereas

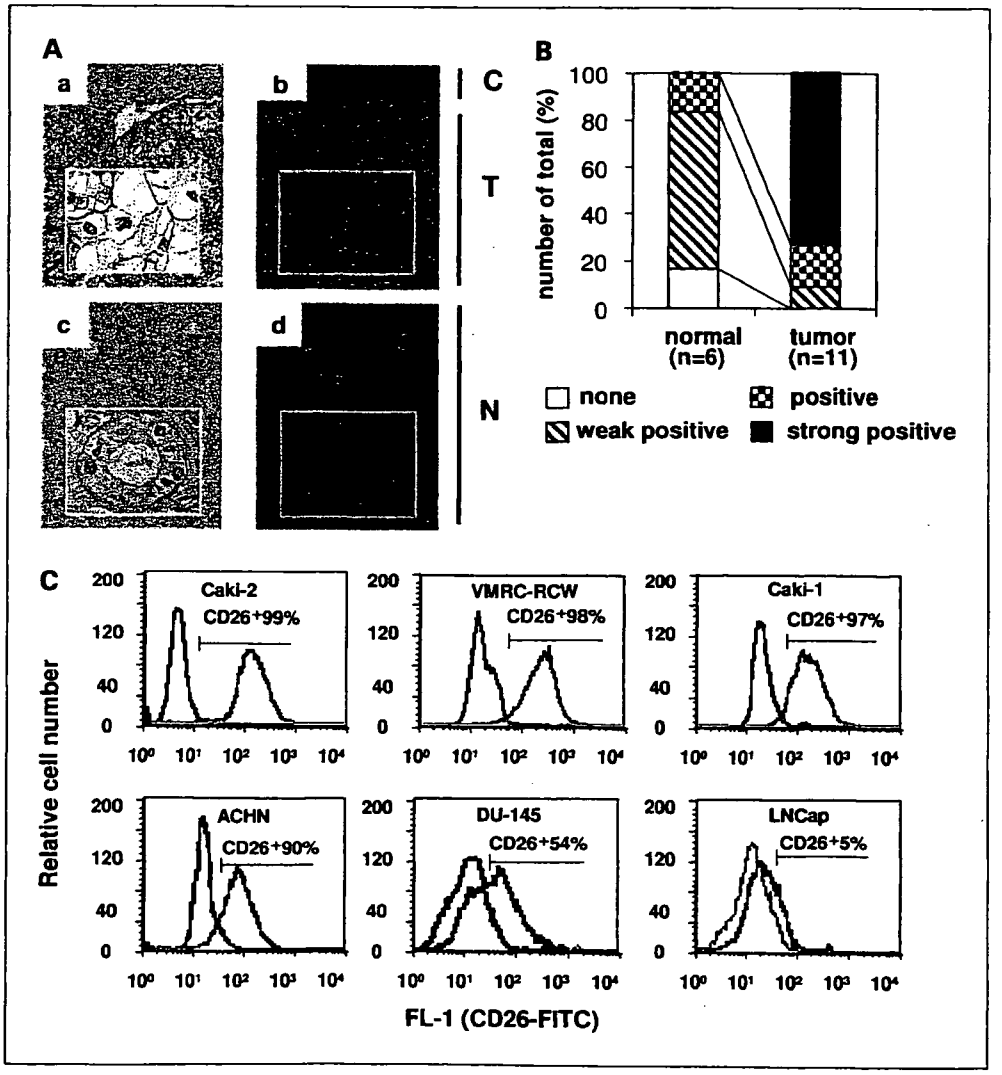

Fig. 1. Cell surface expression of CD26 in human RCC. *A*, immunohistochemical analysis of CD26 expression was done on surgically resected RCC specimens of primary sites. RCC stained with H&E (*a*) and anti-CD26-FITC (*b*). Normal renal structures adjacent to RCC tissues in (*a*) and (*b*) were stained with H&E (*c*) and anti-CD26-FITC (*d*). Representative of 11 consecutive specimens. Original magnification, ×200. *N*, normal renal tissue; *C*, connective tissue; *T*, tumor. *B*, fluorescent intensities of CD26 were evaluated from 11 RCC tissue samples and 6 adjacent normal renal tissues. Fluorescent intensity was determined as follows: strong positive (*T*; Fig. 1A, *b*), positive (Fig. 1A, *d*), weak positive (*C*; Fig. 1A, *b*), or none. Identical experiments were repeated thrice with similar results. *C*, surface expression of CD26 on various cell lines was analyzed by flow cytometry. Red line, CD26 histograms were obtained by staining with mouse anti-CD26 mAb followed by staining with rabbit anti-mouse IgG-FITC conjugate. Black line, control histograms represent background fluorescence obtained by staining of same cell cultures with isotype-matched control mAb.

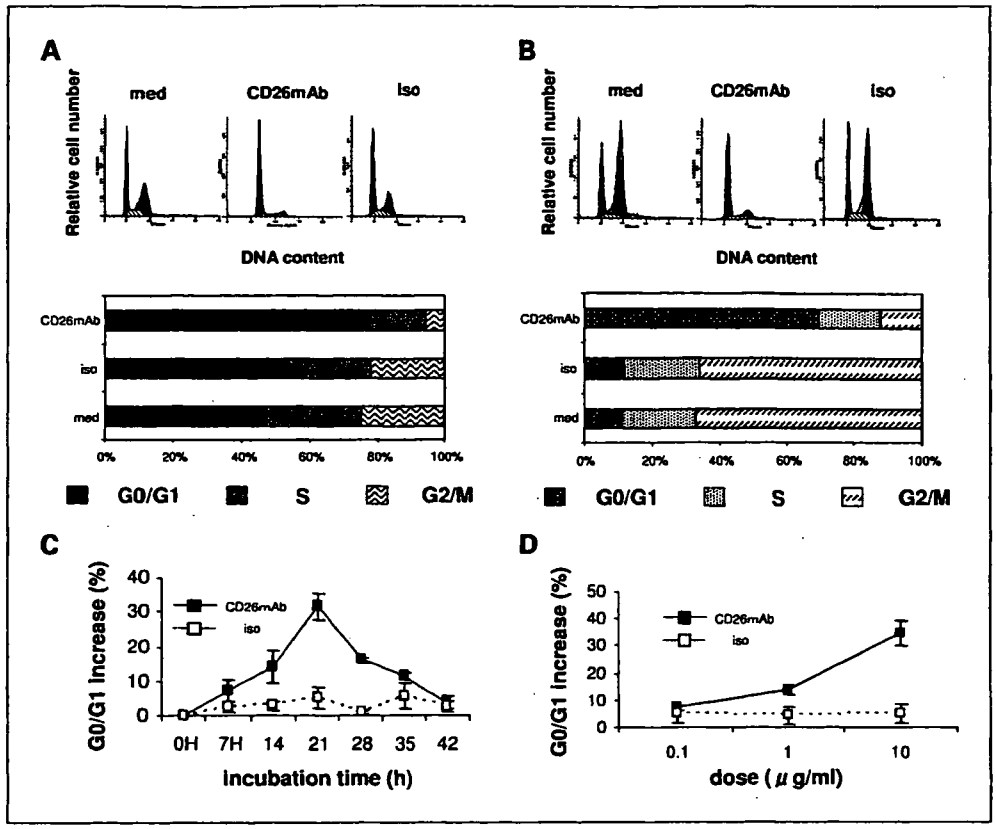

Fig. 2. Anti-CD26 mAb-mediated cell cycle arrest at G_1-S checkpoint in RCC. *A*, Caki-2 cells were treated with medium alone (*med*), anti-CD26 mAb (*CD26mAb*), or isotype-matched control mAb (*iso*) for 21 hours, and cell cycle analysis was done by ModFit program. Histograms were made by CellQuest software. Data are representative of three independent experiments. *B*, nocodazole was added to Caki-2 cells 30 minutes before administration of medium, anti-CD26 mAb, or isotype-matched control mAb. Data are representative of three independent experiments. *C*, Caki-2 cells were treated with isotype-matched control mAb or anti-CD26 mAb. After the indicated time period, cell cycle analysis was done. Points, mean of triplicated tests; bars, SE. *D*, Caki-2 cells were treated with isotype-matched control mAb or anti-CD26 mAb at a concentration of 0.1, 1, and 10 μg/mL. Caki-2 cells were collected for cell cycle analysis at 21 hours after antibody administration.

anti-CD26 mAb-mediated G_0-G_1 arrest occurred in a dose-dependent manner, peaking at 10 μg/mL (Fig. 2D). Consistent with the observed anti-CD26 mAb-induced cell cycle arrest G_1-S, growth of Caki-2, VMRC-RCW, Caki-1, ACHN, and DU-145 cells was inhibited in a dose-dependent manner when treated with anti-CD26 mAb for 24 hours (Fig. 3). However, anti-CD26 mAb had minimal growth-inhibitory effect on LNCap cells, indicating the specific antitumor effect of anti-CD26 mAb.

Enhancement of $p27^{kip1}$ expression, reduction of CDK2, and dephosphorylation of retinoblastoma substrate are associated with anti-CD26 mAb-mediated G_1-S cell cycle arrest through phosphatidylinositol 3-kinase/Akt and ras/raf/MEK/ERK(MAPK) pathways. Because the cell cycle is strictly regulated by regulators (16), we next evaluated the levels of cell cycle regulators in Caki-2 cells following anti-CD26 mAb treatment. Enhanced expression of $p27^{kip1}$, reduction of CDK2, and dephosphorylation of retinoblastoma substrate were observed, with no detectable changes in $p21^{cip/waf1}$, p53, cyclin D1, CDK4, and CDK6 (Fig. 4A). Markedly enhanced $p27^{kip1}$ level was detected in the nuclei of anti-CD26-treated cells (Fig. 4B), corroborated by results of cell fractionation study (Fig. 4C). Moreover, immunoprecipitation analysis with anti-$p27^{kip1}$ mAb revealed that anti-CD26 mAb treatment reduced the amount of phosphothreonine residue of $p27^{kip1}$, suggesting that accumulation of $p27^{kip1}$ is nuclei specific (Fig. 4D; ref. 17). These results strongly suggested that anti-CD26-mediated up-regulation of $p27^{kip1}$ occurred mainly in the nucleus, being potentially responsible for cell cycle arrest in RCC.

Because anti-CD26 mAb induced nuclear accumulation of $p27^{kip1}$ protein, concomitantly reducing the phosphorylated form of $p27^{kip1}$ (Fig. 4B-D), we hypothesized that the phosphatidylinositol 3-kinase/Akt pathway is involved in this process (17, 18). Elucidating the particular signaling pathways involved in anti-CD26 mAb-mediated up-regulation of $p27^{kip1}$, we found that activated Akt was significantly abrogated in Caki-2 cells as early as 7 hours and as late as 21 hours after antibody treatment (Fig. 5A, *b, lanes 16-21*). Attenuation of 44/42MAPK

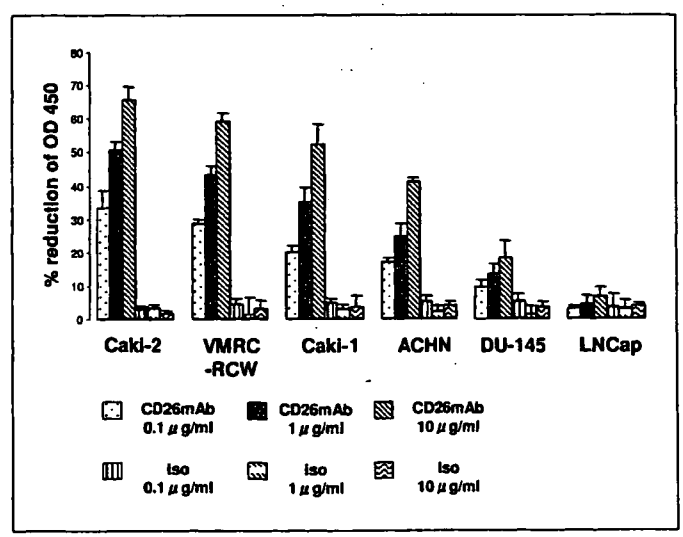

Fig. 3. Inhibitory effect of anti-CD26 mAb on RCC proliferation. Synchronized 5×10^3 cells per well of Caki-2, VMRC-RCW, Caki-1, ACHN, DU-145, and LNCap were incubated in 96-well plates in the presence of either anti-CD26 or isotype-matched control mAbs. After 24 hours of antibody treatment, water-soluble formazan dye on bioreduction in the presence of an electron carrier, 1-methoxy-5-methylphenazinium, was measured at 450 nm using a microplate reader as described in Materials and Methods, and growth-inhibitory ratio was calculated as % reduction of $A_{450\ nm}$.

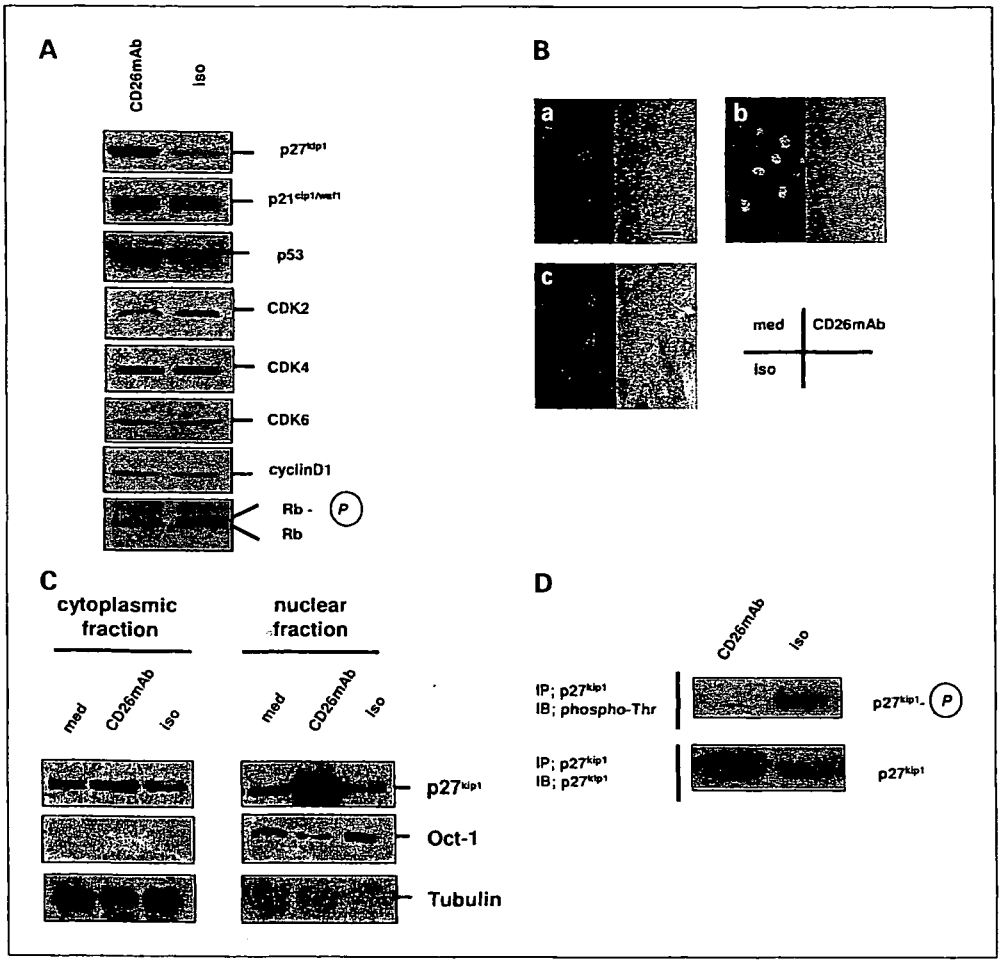

Fig. 4. Anti-CD26 mAb-mediated induction of $p27^{kip1}$ expression. *A*, Caki-2 cells were treated with medium alone, anti-CD26 mAb, or isotype-matched control mAb. At 21 hours after antibody administration, cells were harvested, lysed, subjected to SDS-PAGE, and probed by specific antibody to $p27^{kip1}$, $p21^{cip1/waf1}$, p53, CDK2, CDK4, CDK6, cyclin D1, and phosphorylated retinoblastoma substrate (*Rb*). *B*, Caki-2 cells (5×10^4/mL) were grown on coverslips in six-well plates in medium alone (*a*), anti-CD26 mAb (*b*), or isotype-matched control mAb (*c*). After 21 hours of incubation, cells were subjected to immunocytochemistry as described in Materials and Methods and stained with mouse anti-$p27^{kip1}$ mAb followed by FITC-conjugated anti-mouse IgG. Bar, 50 μm. *C*, after 21 hours of treatment with medium alone, anti-CD26 mAb, or isotype-matched control mAb, Caki-2 cells were harvested for cell fractionation. Each sample was probed with antibodies against $p27^{kip1}$. To determine fractionation purity, Oct-1 and α-tubulin were probed with specific antibodies for cytoplasmic and nuclear fractions, respectively. *D*, for immunoprecipitation, whole-cell lysates were precipitated with anti-$p27^{kip1}$ mAb, subjected to SDS-PAGE, and probed by specific antibody to phosphothreonine.

was also observed as late as 21 hours following antibody treatment of Caki-2 cells (Fig. 5A, *d*, *lanes 19-21*).

To further characterize the specific pathway with a key role in the anti-CD26 mAb-induced enhancement of $p27^{kip1}$ expression, specific inhibitors against each pathway as well as genetically introduced His/Myc-tagged dominant-negative form of Akt (Caki-2-d.n.-Akt) and constitutively active His/Myc-tagged myristylated Akt (Caki-2-myr-Akt) were used (Fig. 5B-D). Caki-2 pretreated with LY294002 (Fig. 5B, *e*, *lanes 3*, *6*, and *9*) and Caki-2-d.n.-Akt (Fig. 5C, *a*, *lanes 7-9*) up-regulated endogenous $p27^{kip1}$ protein level, more importantly resulting in additive up-regulation of $p27^{kip1}$ when combined with anti-CD26 mAb. In contrast, Caki-2-myr-Akt exhibited only sparse basal level of $p27^{kip1}$, completely abolishing anti-CD26 mAb-induced up-regulation of $p27^{kip1}$ (Fig. 5C, *a*, *lanes 10-12*). Meanwhile, PD98059, a specific inhibitor of MEK1, did not cause any detectable change in $p27^{kip1}$ (Fig. 5B, *e*, *lanes 2*, *5*, and *8*). These findings strongly suggested that the phosphatidylinositol 3-kinase/Akt pathway is more potent than the ras/raf/MEK/ERK pathway in mediating anti-CD26 mAb-induced $p27^{kip1}$ accumulation.

To confirm the above results, Caki-2 pretreated with LY294002 and PD98059, Caki-2-d.n.-Akt, and Caki-2-myr-Akt were evaluated for cell proliferation activity. Caki-2 pretreated with LY294002 and Caki-2-d.n.-Akt displayed drastically increased anti-CD26 mAb-mediated growth inhibition, whereas Caki-2-myr-Akt completely abolished this effect (Fig. 5D). On the other hand, pretreatment of Caki-2 with PD98059 did not enhance anti-CD26 mAb-mediated growth inhibition. Taken together, the above results showed that the phosphatidylinositol 3-kinase/Akt pathway was more potent than the ras/raf/MEK/ERK pathway in regulating anti-CD26 mAb-mediated growth arrest and that Akt activity has an effect on anti-CD26 mAb-induced expression of $p27^{kip1}$ and growth arrest.

Anti-CD26 mAb regulates cell adhesion to ECM through internalization of cell surface CD26 and reduces* in vivo *tumorigenicity of Caki-2 associated with prolonged survival. Because CD26 plays a role in cell adhesion to the ECM proteins (19, 20), we examined the effect of anti-CD26 mAb on cellular interaction with the ECM. Anti-CD26 antibody inhibited Caki-2 binding to fibronectin and type I collagen (Fig. 6A) associated with antibody-mediated CD26 internalization (Fig. 6B). These findings thus suggested that contact inhibition may play a contributing role to the observed anti-CD26-mediated up-regulation of $p27^{kip1}$ (21, 22).

We also investigated the effect of anti-CD26 mAb treatment on Caki-2 growth in a xenograft mouse tumor model. Mice treated with anti-CD26 mAb had a lower rate of tumor development than controls, leading to enhanced survival (Fig. 6C). To define the molecular events occurring in inoculated tumors, tumor mass was removed at day 60 after initial treatment for postmortem biochemical analyses of tissue lysates. Our results showed enhanced expression of $p27^{kip1}$ protein with

concomitant inactivation of Akt in the tumor mass (Fig. 6D), consistent with our *in vitro* data (Figs. 4 and 5). Taken together, these results indicated that CD26 may be an appropriate molecular target for RCC therapy.

Discussion

In this study, we show the antitumor effect of anti-CD26 mAb in an *in vitro* and *in vivo* model. Importantly, our study suggests the potential role of CD26 as a molecular target in human RCC, a highly malignant disease that is resistant to standard treatment with chemotherapy or biologics (23). Although highly expressed in RCC, particularly the clear cell type (11), CD26 role in human RCC is poorly understood. Our present results indicate that anti-CD26 mAb induces RCC G_1-S cell cycle and growth inhibition, concomitantly blocking cell adhesion. Our data also suggest that targeting CD26 is a potentially effective therapeutic strategy for selected neoplasms, including human RCC. Of interest is that tumors can result from cell cycle dysregulation, with various cancers expressing low levels of CDK inhibitors, including $p27^{kip1}$ (16).

Although recent work showed that activated Akt regulates both $p27^{kip1}$ subcellular localization and degradation (17, 24), we show that combining anti-CD26 mAb with LY294002 or a dominant-negative form of Akt has an additive effect on $p27^{kip1}$ accumulation. In contrast, constitutively active Akt abolishes not only basal $p27^{kip1}$ protein level but also anti-CD26 mAb-induced $p27^{kip1}$ overexpression, with resultant amelioration of growth inhibition by anti-CD26 mAb. These observed results strongly suggest that Akt negatively regulates total $p27^{kip1}$ protein level, and perturbation of CD26 by its specific antibody engages the same pathway in RCC, leading to an increase in G_0-G_1 phase. Meanwhile, the mechanisms involved in anti-CD26 mAb-induced inactivation of Akt resulting in $p27^{kip1}$ accumulation in RCC remain to be elucidated. One possible explanation may involve the potential interaction between CD26 and the docking sites for Akt. Binding of anti-CD26 antibody causes CD26 internalization, leading to signal transduction. Because Akt is a lipid-binding protein kinase, which becomes activated as a result of recruitment to docking

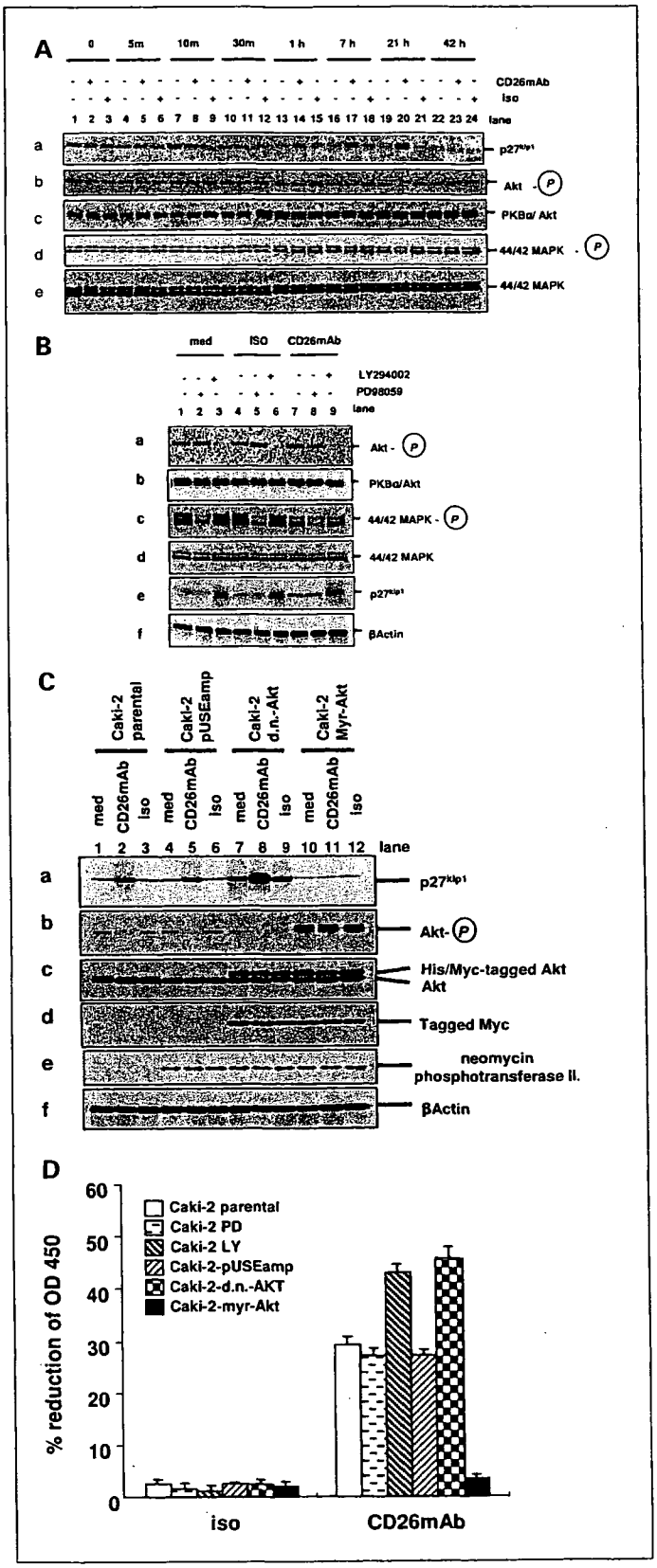

Fig. 5. Anti-CD26 mAb-mediated enhancement of $p27^{kip1}$ in RCC via attenuation of phosphorylated Akt rather than phosphorylated 44/42MAPK. *A*, Caki-2 cells were treated with medium only, anti-CD26 mAb, or isotype-matched control mAb. Caki-2 cells were immediately collected for preparation of whole-cell lysates at 0, 5, 10, and 30 minutes and 1, 7, 21, and 42 hours after administration of indicated panel of antibodies. *B*, for whole-cell lysate preparation, Caki-2 cells were preincubated in the presence or absence of PD98059 and LY294002 30 minutes before treatment with medium alone, isotype-matched control mAb, or anti-CD26 mAb at 10 μg/mL. After 21 hours of antibody treatment, cells were harvested and subjected to SDS-PAGE and immunoblotting for $p27^{kip1}$ (*a*), phosphorylated Akt (*b*), protein kinase Bα/Akt (*c*), phosphorylated 44/42MAPK (*d*), 44/42MAPK (*e*), and β-actin (*f*). *C*, SDS-PAGE and immunoblotting of whole-cell lysates of Caki-2 cells that express a His/Myc-tagged dominant-negative Akt (Caki-2-d.n.-Akt), His/Myc-tagged myristylated constitutively active Akt (Caki-2-myr-Akt), and control vector (Caki-2-pUSEamp). Transient transfectants of Caki-2-pUSEamp, Caki-2-d.n.-Akt, and Caki-2-myr-Akt were made, and after 48 hours, each of the three transfectants was treated by medium alone, 10 μg/mL anti-CD26 mAb, or 10 μg/mL isotype-matched control mAb. Twenty-one hours after antibody treatment, cells were collected, lysed, subjected to SDS-PAGE and immunoblotting, and probed with specific antibody to $p27^{kip1}$ (*a*), phosphorylated Akt (*b*), protein kinase Bα/Akt (*c*), Myc (*d*), neomycin phosphotransferase II (*e*), and β-actin (*f*). *D*, *in vitro* proliferation assay of Caki-2-parental, Caki-2 pretreated by PD98059, Caki-2 pretreated by LY294002, Caki-2-pUSEamp, Caki-2-d.n.-Akt, and Caki-2-myr-Akt. Caki-2 cells were preincubated in the presence or absence of PD98059 (*Caki-2 PD*) and LY294002 (*Caki-2 LY*) for 30 minutes before treatment with isotype-matched control or anti-CD26 mAbs. Transient transfectants of Caki-2-pUSEamp, Caki-2-d.n.-Akt, and Caki-2-myr-Akt were established 48 hours before treatment with isotype-matched control mAb or anti-CD26 mAb. Anti-CD26 and isotype-matched control mAbs were administered at 10 μg/mL to each cell type, and then cells were subjected to *in vitro* cell proliferation assay. Independent tests were examined in triplicates. Columns, mean; bars, SE.

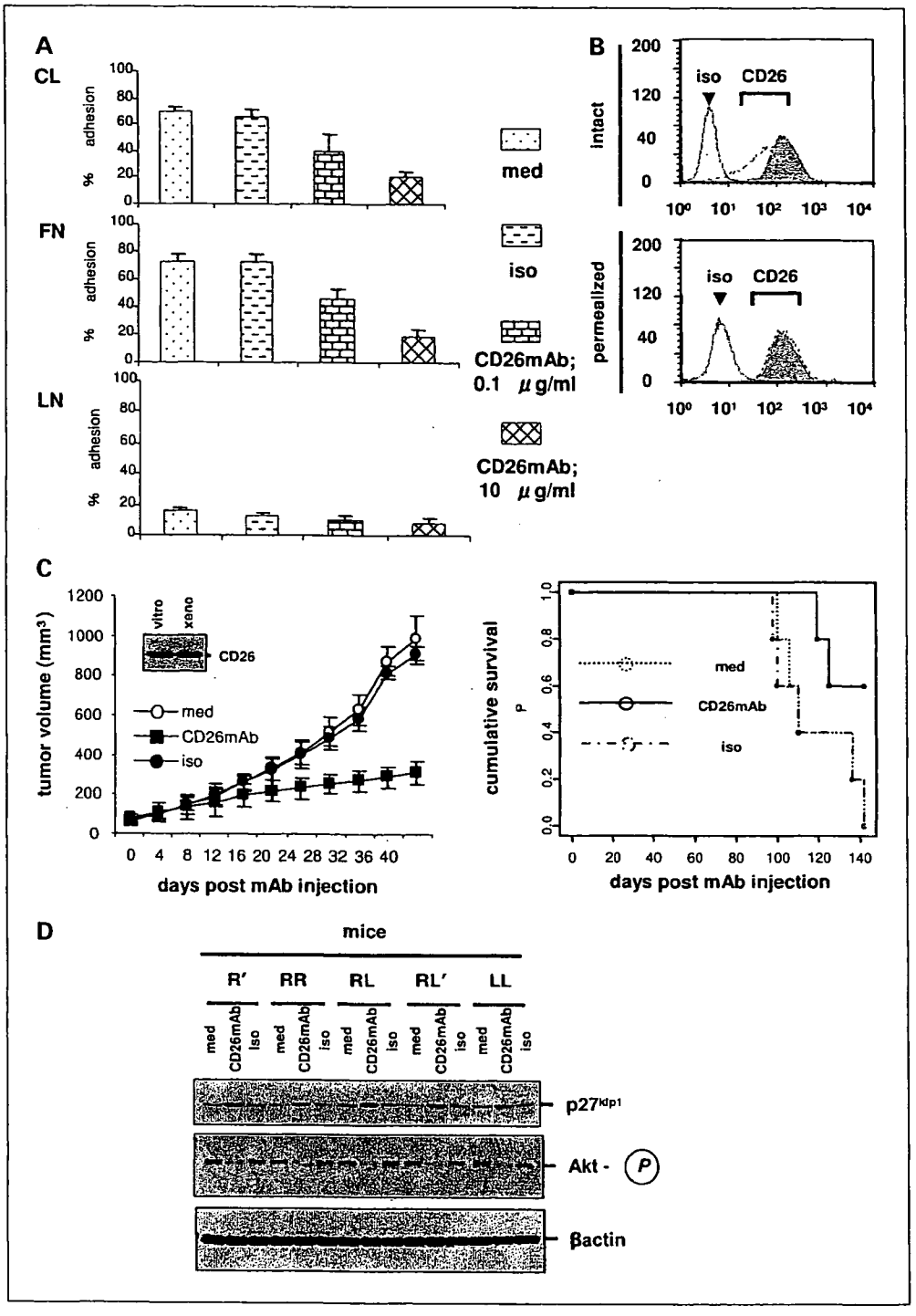

Fig. 6. Antitumor effect of anti-CD26 mAb in mouse xenograft model of Caki-2. *A*, effect of anti-CD26 mAb on cell adhesion to ECM. Caki-2 cells treated with medium only, anti-CD26 mAb, or isotype-matched control mAb were plated onto 60-mm dishes (3×10^6 per dish) coated with collagen I (*CL*), fibronectin (*FN*), or laminin (*LN*) and cultured for 21 hours. The adhesive ability of cancer cells was expressed as the mean number of cells that had attached to the bottom surface of the dish. Columns, mean number of cells per field of view; bars, SE. Values for invasion were determined by calculating the average number of adhesive cells per mm^2 over three fields per assay and expressed as an average of triplicate determinations. Adhesive cells (%): adhesive cells / adhesive cells + nonadhesive cells. *B*, Caki-2 cells were treated with anti-CD26 mAb on ice, or isotype-matched control mAb, followed by washing in ice-cold PBS twice and subsequently incubated at 37°C for 12 hours. Cell were collected and stained with FITC-conjugated anti-mouse IgG. Expression status of cell surface CD26 was analyzed by flow cytometry. To detect total CD26 level, including the internalized CD26 fraction, cell membrane permeabilization method was used (26). Filled histogram, positive control, which was incubated 30 minutes with anti-CD26 mAb. Open histogram, status of CD26 after treatment. *C*, Caki-2 cells (1×10^6) were inoculated s.c. into the left flank of mice. CD26 expression of Caki-2 cells after tumor implantation into the mouse was similar to its level before tumor implantation. Mice were treated with intratumoral injection of PBS only (medium; $n = 5$), anti-CD26 mAb ($n = 5$), or isotype-matched control mAb ($n = 5$) on the day when the tumor mass became visible (5 mm in size). Tumor size and cumulative survival were monitored. *D*, resected specimens were immediately frozen for whole-cell lysate preparation and lysed by lysis buffer as described in Materials and Methods. Protein (50 μg) was applied for SDS-PAGE and immunoblotting for $p27^{kip1}$, phosphorylated Akt, and β-actin. R', RR, RL, RL', and LL, names of mice in each treatment group.

sites consisting of phosphatidylinositol phosphate in the plasma membrane (25), antibody-induced CD26 internalization may affect Akt docking and activation in RCC. Moreover, because anti-CD26 mAb blocks ECM binding and because $p27^{kip1}$ is up-regulated during contact inhibition (21), anti-CD26 mAb may induce cellular mechanisms associated with contact inhibition in selected CD26-positive adhesive tumors.

Our present study shows that CD26 is highly expressed in human RCC and that anti-CD26 mAb binding engages key signaling pathways, resulting in G_1-S arrest. Our subsequent *in vivo* experiments further indicate that CD26 is an appropriate molecular target for RCC therapy by showing that anti-CD26 mAb treatment leads to loss of tumorigenicity. We postulate that the potent antitumor effect of anti-CD26 mAb observed in our study may be used in the future as novel therapeutic approaches against various CD26-positive malignancies, including RCC.

Acknowledgments

We thank Y. Urasaki and Y. Itoh for their technical assistance.

References

1. Morimoto C, Schlossman SF. The structure and function of CD26 in the T-cell immune response. Immunol Rev 1998;161:55–70.
2. Ishii T, Ohnuma K, Murakami A, et al. CD26-mediated signaling for T cell activation occurs in lipid rafts through its association with CD45RO. Proc Natl Acad Sci U S A 2001;98:12138–43.
3. Ohnuma K, Yamochi T, Uchiyama M, et al. CD26 up-regulates expression of CD86 on antigen-presenting cells by means of caveolin-1. Proc Natl Acad Sci U S A 2004;101:14186–91.
4. Yamochi T, Yamochi T, Aytac U, et al. Regulation of p38 phosphorylation and topoisomerase IIα expression in the B-cell lymphoma line Jiyoye by CD26/dipeptidyl peptidase IV is associated with enhanced *in vitro* and *in vivo* sensitivity to doxorubicin. Cancer Res 2005;65:1973–83.
5. Ohnuma K, Ishii T, Iwata S, et al. G_1/S cell cycle arrest provoked in human T cells by antibody to CD26. Immunology 2002;107:325–33.
6. Ho L, Aytac U, Stephens LC, et al. *In vitro* and *in vivo* antitumor effect of the anti-CD26 monoclonal antibody 1F7 on human $CD30^+$ anaplastic large cell T-cell lymphoma Karpas 299. Clin Cancer Res 2001;7:2031–40.
7. Pro B, Dang NH. CD26/dipeptidyl peptidase IV and its role in cancer. Histol Histopathol 2004;19:1345–51.
8. Iwata S, Morimoto C. CD26/dipeptidyl peptidase IV in context. The different roles of a multifunctional ectoenzyme in malignant transformation. J Exp Med 1999;190:301–6.
9. Kehlen A, Lendeckel U, Dralle H, Langner J, Hoang-Vu C. Biological significance of aminopeptidase N/CD13 in thyroid carcinomas. Cancer Res 2003;63:8500–6.
10. Kajiyama H, Kikkawa F, Suzuki T, Shibata K, Ino K, Mizutani S. Prolonged survival and decreased invasive activity attributable to dipeptidyl peptidase IV overexpression in ovarian carcinoma. Cancer Res 2002;62:2753–7.
11. Droz D, Zachar D, Charbit L, Gogusev J, Chrétein Y, Iris L. Expression of the human nephron differentiation molecules in renal cell carcinomas. Am J Pathol 1990;137:895–905.
12. Morimoto C, Torimoto Y, Levinson G, et al. 1F7, a novel cell surface molecule, involved in helper function of CD4 cells. J Immunol 1989;143:3430–9.
13. Kobayashi S, Ohnuma K, Uchiyama M, et al. Association of CD26 with CD45RA outside lipid rafts attenuates cord blood T-cell activation. Blood 2004;103:1002–10.
14. Blajeski AL, Phan VA, Kottke TJ, Kaufmann SH. G(1) and G(2) cell-cycle arrest following microtubule depolymerization in human breast cancer cells. J Clin Invest 2002;110:91–9.
15. Sato K, Aytac U, Yamochi T, et al. CD26/dipeptidyl peptidase IV enhances expression of topoisomerase IIα and sensitivity to apoptosis induced by topoisomerase II inhibitors. Br J Cancer 2003;89:1366–74.
16. Sherr CJ. Principles of tumor suppression. Cell 2004;116:235–46.
17. Shin I, Yakes FM, Rojo F, et al. PKB/Akt mediates cell-cycle progression by phosphorylation of p27 (Kip1) at threonine 157 and modulation of its cellular localization. Nat Med 2002;8:1145–52.
18. Viglietto G, Motti ML, Bruni P, et al. Cytoplasmic relocalization and inhibition of the cyclin-dependent kinase inhibitor p27(Kip1) by PKB/Akt-mediated phosphorylation in breast cancer. Nat Med 2002;8:1136–44.
19. Cheng HC, Abdel-Ghany M, Pauli BU. A novel consensus motif in fibronectin mediates dipeptidyl peptidase IV adhesion and metastasis. J Biol Chem 2003;278:24600–7.
20. Dang NH, Torimoto Y, Schlossman SF, Morimoto C. Human CD4 helper T cell activation: functional involvement of two distinct collagen receptors, 1F7 and VLA integrin family. J Exp Med 1990;172:649–52.
21. Suzuki E, Nagata D, Yoshizumi M, et al. Reentry into the cell cycle of contact-inhibited vascular endothelial cells by a phosphatase inhibitor. Possible involvement of extracellular signal-regulated kinase and phosphatidylinositol 3-kinase. J Biol Chem 2000;275:3637–44.
22. Levenberg S, Yarden A, Kam Z, Geiger B. p27 is involved in N-cadherin-mediated contact inhibition of cell growth and S-phase entry. Oncogene 1999;18:869–76.
23. Vogelzang NJ, Stadler WM. Kidney cancer. Lancet 1998;352:1691–6.
24. Medema RH, Kops GJ, Bos JL, Burgering BM. AFX-like Forkhead transcription factors mediate cell-cycle regulation by Ras and PKB through p27kip1. Nature 2000;404:782–7.
25. Luo J, Manning BD, Cantley LC. Targeting the PI3K-Akt pathway in human cancer: rationale and promise. Cancer Cell 2003;4:257–62.
26. Suyama K, Shapiro I, Guttman M, Hazan RB. A signaling pathway leading to metastasis is controlled by N-cadherin and the FGF receptor. Cancer Cell 2002;2:301–14.

Mod Rheumatol (2006) 16:3–13
DOI 10.1007/s10165-005-0452-4

REVIEW ARTICLE

**Kei Ohnuma · Hiroshi Inoue · Masahiko Uchiyama
Tadanori Yamochi · Osamu Hosono · Nam H. Dang
Chikao Morimoto**

T-cell activation via CD26 and caveolin-1 in rheumatoid synovium

Received: September 13, 2005 / Accepted: December 16, 2005

Abstract CD26 is a T-cell costimulatory molecule with dipeptidyl peptidase IV (DPPIV) activity in its extracellular region. We previously reported that recombinant soluble CD26 enhances peripheral blood T-cell proliferation induced by the recall antigen tetanus toxoid (TT). Recently, we demonstrated that CD26 binds caveolin-1 on antigen-presenting cell (APC), and that residues 201–211 of CD26 along with the serine catalytic site at residue 630, which constitute a pocket structure of CD26/DPPIV, contribute to binding to caveolin-1 scaffolding domain. In addition, following CD26–caveolin-1 interaction on TT-loaded monocytes, caveolin-1 is phosphorylated, with linkage to NF-κB activation, followed by upregulation of CD86. Finally, reduced caveolin-1 expression on APC inhibits CD26-mediated CD86 upregulation and abrogates CD26 effect on TT-induced T-cell proliferation, and immunohistochemical studies revealed an infiltration of CD26+ T cells in the sublining region of rheumatoid synovium and high expression of caveolin-1 in the increased vasculature and synoviocytes of the rheumatoid synovium. Taken together, these results strongly suggest that CD26–cavolin-1 interaction plays a role in the upregulation of CD86 on TT-loaded APC and subsequent engagement with CD28 on T cells, leading to antigen-specific T-cell activation such as the T-cell-mediated antigen-specific response in rheumatoid arthritis.

Key words Caveolin-1 · CD26 · Memory T cell · Rheumatoid arthritis (RA) · Synovial cell

K. Ohnuma · M. Uchiyama · T. Yamochi · O. Hosono · C. Morimoto (✉)
Department of Clinical Immunology, Advanced Clinical Research Center, Institute of Medical Science, University of Tokyo, 4-6-1 Shirokanedai, Minato-ku, Tokyo 108-8639, Japan
Tel. +81-354-495-546; Fax +81-354-495-448
e-mail: morimoto@ims.u-tokyo.ac.jp

H. Inoue
Inoue Hospital, Takasaki, Japan

N.H. Dang
Department of Hematologic Malignancies, Nevada Cancer Institute, Las Vegas, NV 89135, USA

Introduction

Rheumatoid arthritis (RA) is a chronic inflammatory disease characterized by the progressive destruction of cartilage and bone in the synovial joints, which is associated with proliferation of synovial cells and infiltration of activated memory T cells, antigen-presenting cells (APCs) and plasma cells.[1] Proposed etiologies for RA include genetic predisposition, dysregulation of self-tolerance, immune dysregulation triggered by environmental agents, and subsequent transformation of synovial cells.[1–3] Macrophages and/or T cells are important mediators of RA pathogenesis, with cytokines such as tumor necrosis factor alpha (TNF-α) and interleukin-1 (IL-1) being proven therapeutic targets. In fact, antagonists against such cytokines have been used recently as effective RA therapy, decreasing joint damage and slowing radiographic progression of disease in patients of RA with inadequate response to methotrexate.[4–7] However, as many patients do not experience effective relief even with the use of these newer biological agents, additional novel therapeutic approaches are still needed.[8–10]

Major-histocompatibility-complex (MHC) class II phenotype such as HLA-DR1, DR-4 and DR-14 confers susceptibility to RA.[11–14] MHC class II molecules present antigens to CD4+ T cells, suggesting an important role for T cells in the pathogenesis of RA. Moreover, the rheumatoid synovium contains activated T cells, providing further rationale for the proposal that T cells have an important role in RA.[15,16] Antigen-presenting cells such as monocytes, macrophages, and dendritic cells are also present in the rheumatoid synovium,[1] being activated and expressing both MHC class II and costimulatory molecules such as CD86 and CD80. These findings strongly suggest that the interaction between synovial T cells and APCs have a direct role in the progression of synovitis.[2] Moreover, careful analysis of infiltrating synovial T cells has revealed a bias towards the T_H1 phenotype.[17,18] In particular, patients with autoimmune diseases such as multiple sclerosis, Graves' disease, and RA have been found to have increased numbers of CD4+

CD26+ T cells in inflamed tissues as well as in their peripheral blood,[19-22] with enhancement of CD26 expression in these autoimmune diseases correlating with disease severity.[19,20,23] In addition, we previously demonstrated that T cells migrating through endothelial cell monolayers in vitro express high levels of CD26.[24] These findings imply that CD26+ T cells play an important role in the inflammation process and subsequent tissue damage in such diseases.

It is well established that T cells require at least two signals to be fully activated.[25] The first signal is antigen-specific and is delivered by engagement of the T-cell receptor (TCR) complex with an MHC-peptide complex on APC. The second signal is exerted by the binding of a costimulatory receptor on T cells to a ligand on the APCs. A key costimulatory signal is provided by the interaction of CD28 on T cells with CD86 or CD80 on APCs. We showed previously that CD26 on T cells have a very strong costimulatory effect on CD4+ T-cell activation in response to memory antigen such as tetanus toxoid (TT).[26-29] However, the molecular mechanism involved in the process of antigen-specific T-cell activation via CD26 has not been clearly elucidated. We recently demonstrated that caveolin-1 on antigen-loaded monocytes is a binding partner of CD26 and that signaling downstream of caveolin-1 in APC is triggered by stimulation with exogenous CD26.[30,31] Therefore, T-cell costimulation via CD26 as well as CD28 may have an important role in the pathophysiology of inflammatory diseases such as RA. In this review, we discuss various aspects of CD26 involvement in immune regulation and immune-mediated disorders such as RA, with a particular focus on the role of caveolin-1 as its key binding partner.

Structure and function of CD26

CD26 is a 110kDa cell-surface glycoprotein that belongs to the serine protease family, and human CD26 is expressed on a variety of tissues including T lymphocytes, endothelial and epithelial cells. As shown in Fig. 1A, human CD26 is composed of 766 amino acids, including a short cytoplasmic domain of 6 amino acids, a transmembrane region of 24 amino acids, and an extracellular domain with dipeptidyl peptidase activity which selectively removes the N-terminal dipeptide from peptides with proline or alanine at the penultimate position (dipeptidyl peptidase IV, DPPIV).[32] The amino acid sequence of human CD26 illustrates approximately 85% homology with the rat DPPIV enzyme and the mouse thymocyte activation molecule (THAM), the mouse homologue of human CD26.[33] CD26 knockout (CD26-KO) mice with C57BL/6 background display an apparently normal phenotype.[34,35] However, the percentage of CD4+ T cells is lower in the spleen lymphocyte population in the CD26-KO mice than in CD26-positive wild-type mice. After immunization of mice with PWM in vivo, serum levels of total IgG, IgG_1, IgG_{2a} and IgE were markedly decreased in CD26-KO mice than those in wild-type mice. Moreover, IL-4 and IL-2 level in sera of CD26-KO mice were decreased and production of interferon-gamma (IFN-γ) was delayed in response to PWM immunization. These results indicate that CD26 helps to regulate the development, maturation and migration of CD4+ T lymphocytes, cytokine secretion, T cell-dependent antibody production, and immunoglobulin isotype switching of B cells.[34]

In contrast to the function of murine CD26, human CD26+ T cells exert diverse effects.[28,36,37] CD26 is a membrane-associated ectopeptidase with DPPIV activity, and possible substrates of CD26/DPPIV include several critical cytokines and chemokines. Activity of RANTES (regulated on activation, normal T-cell expressed and secreted; CCL5) is altered by the enzymatic cleavage of DPPIV, as CD26/DPPIV-processed RANTES affects important activities such as those implicated in monocyte chemotaxis and HIV-1 infection.[38,39] Other important chemokines that appear to be substrates of DPPIV enzymatic activity include eotaxin (CCL11), macrophage-derived chemokine (MDC) (CCL22), interferon inducible chemokines (CXCL10), and other chemokines involved in the inhibition of HIV infection.[39] In addition, recent work showed that CD26 plays an important role in the mobilization of hematopoietic stem cell (HSC) and hematopoietic progenitor cells (HPC) induced by granulocyte colony-stimulating factor (G-CSF).[40] One of the substrates of CD26/DPPIV is CXCL12 (SDF-1α, stromal cell-derived factor 1 alpha), an important chemokine that serves as a chemoattractant for HSC/HPC.[41,42] It has been shown that CXCL12 can be selectively truncated in vitro by CD26/DPPIV, and the truncated molecule lacks the ability to induce migration of hematopoietic cells isolated from mouse bone marrow. Furthermore, treatment of mice with CD26/DPPIV inhibitors during the process of G-CSF mobilization results in a significant reduction in the number of mobilized HPC.[40,41] Other exciting development regarding DPPIV involves its role in glucose metabolism, since inhibition of endogenous glucagon-like peptide 1 (GLP-1) degradation by reducing DPPIV activity is an alternative strategy for improving the incretin action of GLP-1 in vivo and regulating glucose levels.[43] Selective small molecule inhibitors of DPPIV are currently being investigated in clinical trials for the treatment of impaired glucose tolerance and type 2 diabetes.[44]

Besides its ability to regulate the effect of biological factors through DPPIV enzyme activity, CD26 has an essential role in human T-cell physiology, especially in response to memory antigens (Fig. 1B).[28] Originally characterized as a T-cell differentiation antigen, CD26 is preferentially expressed on a specific population of T lymphocytes, the subset of CD4+ CD45RO+ memory T cells, and is upregulated following T-cell activation.[29] Besides being a marker of T-cell activation, CD26 is also associated with T-cell signal transduction processes as a costimulatory molecule.[27,37,45,46] In addition, CD26 serves as a functional collagen receptor with a role in T-cell activation, as well as having a potential role in thymic ontogeny (Fig. 2).[26,46,47] The enzymatic activity of CD26 appears to be very important in enhancing cellular responses to external stimuli. For example, Jurkat cells transfected with wild type CD26 consis-

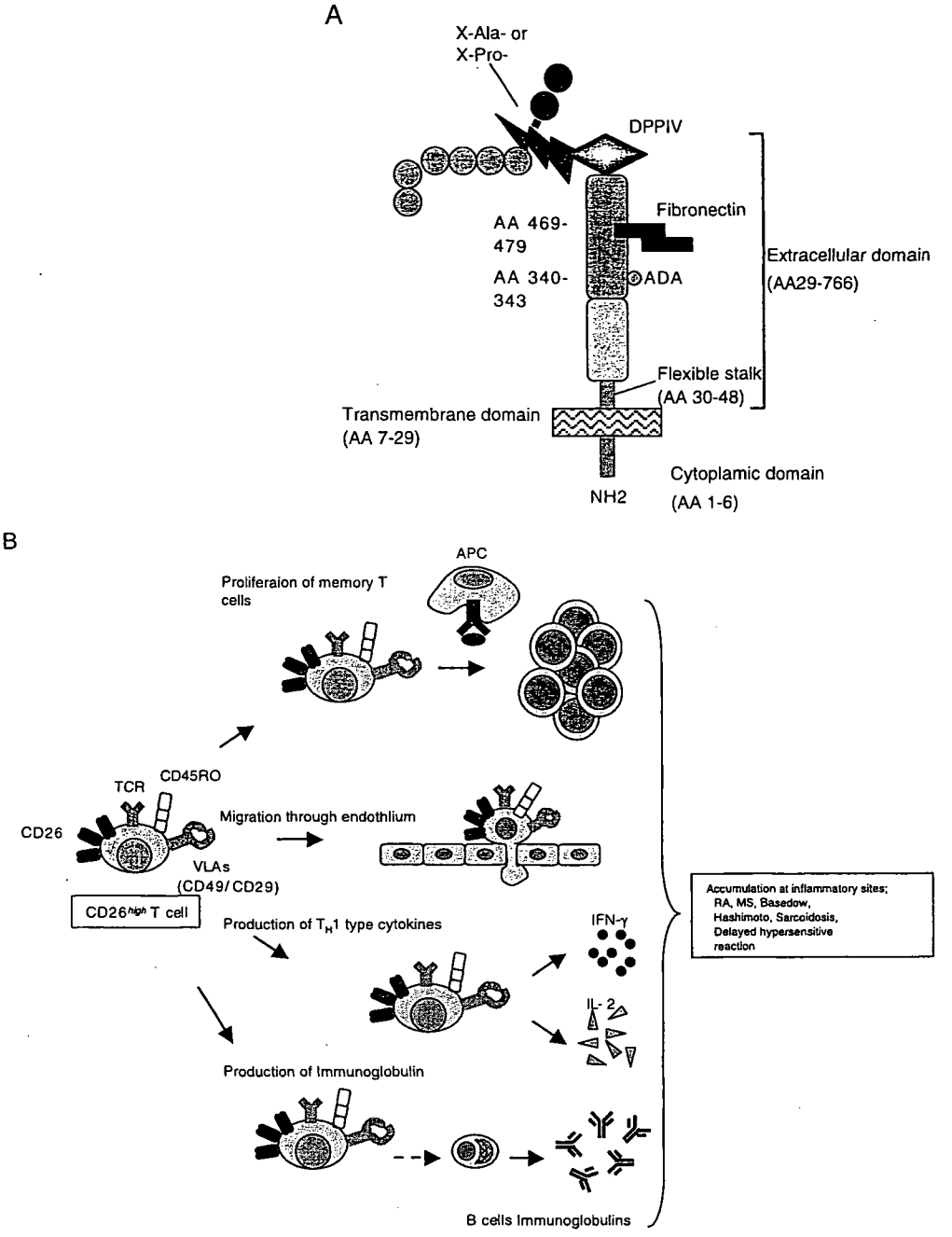

Fig. 1. **A** Schematic diagram of human CD26 structure. Adenosine deaminase (*ADA*) binding site at residues 340–343, fibronectin binding site at residue 469–479, and dipeptidyl peptidase IV (*DPPIV*) enzyme activity at Ser630. *X-Ala-* or *X-Pro-* denotes peptides containing any amino acid at N-terminal position with alanine or proline at the penultimate position. **B** Cellular function of $CD26^{high}$ T cell. See text for details. *APC*, antigen-presenting cell; *TCR*, T-cell receptor; *IFN*, interferon; *IL*, interleukin

tently demonstrate greater activation than parental CD26 negative Jurkat or cells transfected with CD26 mutated at the DPPIV enzymatic site.[48] Furthermore, CD26 interacts with several molecules playing important roles in T-cell function. CD26 physically binds with adenosine deaminase (ADA), an enzyme that plays a key role in the development and function of lymphoid tissues.[49–51] Adenosine deaminase is essential for purine metabolism, with the loss of ADA leading to a clinical syndrome characterized by severe immunodeficiency.[52] When the ADA inhibitor pentostatin was used in the treatment of recurrent T-cell lymphomas, a significant reduction in circulating CD26+ T cells was observed in treated patients.[53] This finding is consistent with the fact that there is a physical association between CD26 and ADA on the surface of T lymphocytes. CD26 also interacts with CD45RO, a tyrosine phosphatase with a critical role in T-cell signal transduction, at lipid rafts in peripheral blood T lymphocytes to modify cellular signaling events (Fig. 2).[54,55] Interestingly, CD26 is associated with CD45 RA outside of lipid rafts in cord blood T cells, and the strong physical linkage of CD26 and CD45 RA may be responsible for the attenuation of cord blood T-cell activation signaling through CD26, which may in turn result in immature immune response and the relatively low incidence of severe graft-versus-host disease (GVHD) in cord blood transplantation (Fig. 2).[56]

Since the 1970s, DPPIV-like activity has been reported in human serum. After identification of the ADA-binding

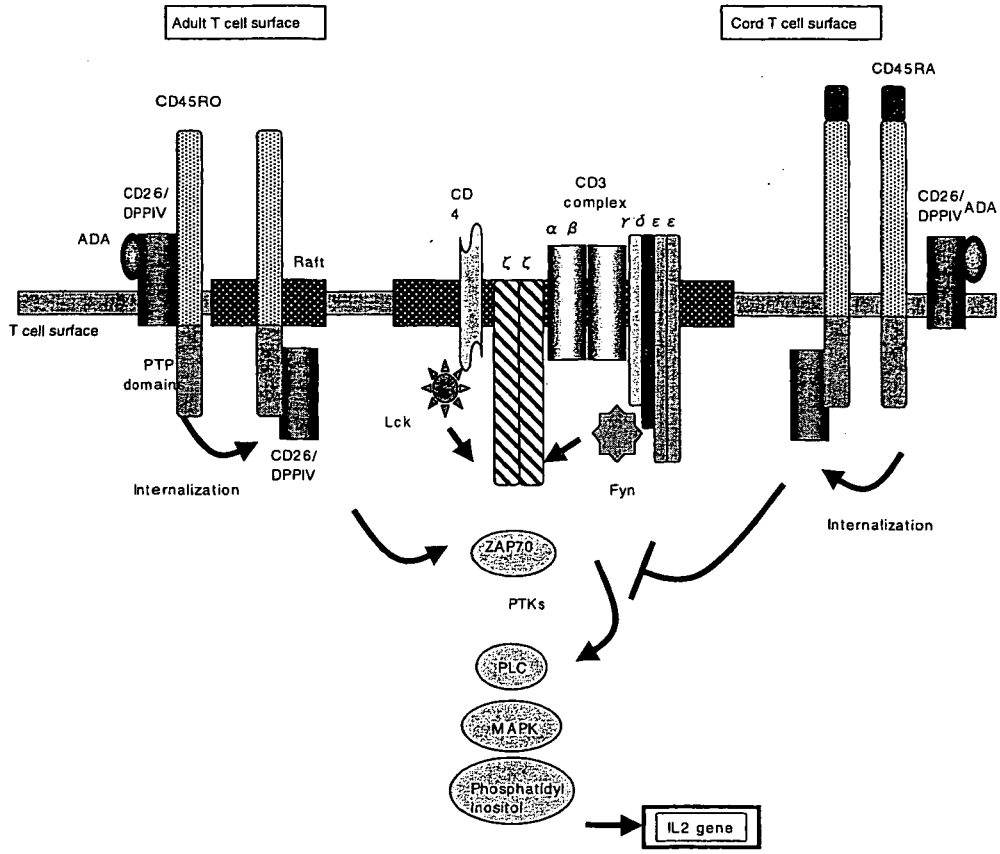

* the diagrams and models of molecules are not to scale.

Fig. 2. Schematic diagram of CD26-associated molecules in T-cell receptor-mediated activation of human adult peripheral blood T cell and cord blood T cell

protein of plasma as CD26, soluble form of CD26 protein was characterized in the serum and seminal fluids.[57,58] In the previous report, we have shown that exogenous recombinant soluble CD26 (rsCD26) enhances the proliferative response of peripheral blood lymphocytes (PBLs) to stimulation with the soluble antigen tetanus toxoid (TT).[59] More recently, we demonstrated that the target cells of rsCD26 are the CD14+ monocytes in the peripheral blood, and that rsCD26 upregulates CD86 expression, but not CD80 or HLA-DR antigen levels on monocytes.[30] Significantly, mannose 6-phosphate/insulin-like growth factor II receptor (M6P/IGF-IIR) was identified as a platform molecule for CD26 interaction with APC.[30] However, while both DPPIV-positive and DPPIV-negative rsCD26 are taken up by monocytes via M6P/IGF-IIR, only DPPIV-positive rsCD26 molecules affect CD86 upregulation on monocytes, thus suggesting that additional key factors may interact with CD26 in this process. We subsequently identified caveolin-1 on APC as a binding protein for CD26, and demonstrated that CD26 stimulation upregulates surface expression of CD86 on APC by means of caveolin-1 and enhances TT-mediated T-cell proliferation.[31] In the next section of this review, we will focus on caveolin-1 as the binding protein of CD26 in the context of antigen-driven T-cell activation.

Structure and function of caveolin-1

Caveolin-1 was the first family member discovered, and demonstrated as a structural component and marker for caveolae and trans-Golgi derived transport vesicles.[60,61] Caveolae were described as structures resembling "little caves" due to their appearance as 50- to 100-nm vesicular invaginations of the plasma membrane.[62] Caveolin-1 is expressed in a wide variety of cell types, especially terminally differentiated cells such as endothelial cells, adipocytes, alveolar type I pneumocytes, macrophages, synoviocytes, and smooth muscle cells. Presently, caveolin-related proteins have been identified as caveolin-1, -2, and -3, all of which serve as protein markers for caveolae.[63] The majority of caveolae in cells and tissues require only caveolin-1 expression for their proper formation, whereas caveolin-2 is not absolutely required, although the expression of caveolin-2 is tightly associated with the expression of caveolin-1.[64,65] On the other hand, caveolin-3 is found in skeletal muscle tissue and cardiac myocytes.[66] The three human genes encoding members of the caveolin family share significant homology. The caveolin-2 protein is approximately 38% identical and 58% similar to caveolin-1, while caveolin-3 is more closely related to caveolin-1, with 65% identity and 85% similarity.[63] All three caveolins possess an invariant "FEDVIAEP" stretch within their hydrophilic N-terminal domains which